NOVA SCHOOL OF SCIENCE & TECHNOLOGY

DEPARTAMENT OF
MECHANICAL AND INDUSTRIAL ENGINEERING

José Miguel Lourenço das Neves
BSc in Mechanical Engineering

Deposition and characterization of AZ61A Magnesium alloy in GMAW-based WAAM

MASTER IN MECHANICAL ENGINEERING
NOVA University Lisbon
September, 2022

NOVA SCHOOL OF SCIENCE & TECHNOLOGY

DEPARTAMENT OF
MECHANICAL AND INDUSTRIAL ENGINEERING

Deposition and Characterization of AZ61A Magnesium alloy in GMAW-based WAAM.

JOSÉ MIGUEL LOURENÇO DAS NEVES

BSc in Mechanical Engineering

Adviser: João Pedro Oliveira
Invited Assistant Professor, NOVA University Lisbon

Examination Committee:

Chair: Telmo Jorge Gomes dos Santos,
Associate Professor with Habilitation, NOVA University Lisbon

Rapporteurs: Valdemar Rebelo Duarte,
Invited Assistant Professor, NOVA University Lisbon

Adviser: João Pedro Oliveira,
Assistant Professor, NOVA University Lisbon

MASTER'S IN MECHANICAL ENGINEERING

NOVA University Lisbon
September 2022

Deposition and Characterization of AZ61A Magnesium alloy in GMAW-based WAAM

To my family

ACKNOWLEDGMENTS

Throughout my project I've come to realize the importance of collaboration and communication, I could not have completed this thesis alone. I will now address the acknowledgments.

Firstly, to my supervisor, Professor João Pedro Oliveira for his availability and expertise. Professor João always showed great patience and confidence in me inspiring me to be more responsible and proactive throughout the project.

To Mr. António Campos and Mr. Paulo Magalhães for their availability to assist with workshop tasks and always teaching me more than I could have expected.

To Maria Morais for the availability to conduct the X-ray diffraction characterization of the samples.

To Tiago Rodrigues and Valdemar Duarte for their availability to teach me about the systems they developed and their helpful ideas.

To all my colleagues at the laboratory for their help on a day-to-day basis and their companionship.

To my dear friends: Igor Felice, Rui Gonçalves, and Lukas Theis for their friendship and expertise, each in their own way. Their willingness to be involved in my project and continuous support was of great importance.

I am also extremely grateful for my group of friends who like to stay in the shade and do as little as possible, the Alentejanos, and to my pal, my homeboy, my rotten soldier, Rúben Branco. It was a long journey but even in the end, we managed to support each other.

To my incredible girlfriend, Patrícia Taborda, for holding me to higher standards than I hold myself. For always helping me view things differently and for teaching me so much about research, fish, and life.

To my family. To my sisters and parents for always supporting me and being interested in my project.

This activity has received funding from the European Institute of Innovation and Technology (EIT) – Project Smart WAAM: Microstructural Engineering and Integrated Non-Destructive Testing. This body of the European Union receives support from the European Union's Horizon 2020 research and innovation program.

Abstract

Additive Manufacturing (AM) is considered an integral part of the 4th Industrial Revolution, allowing breakthroughs in each step of production. In this category, Direct Energy Deposition processes like Wire and Arc Additive Manufacturing (WAAM) have shown capability of high deposition rates, the ability to produce large parts while being economically advantageous. However, many typical defects such as pores and cracks and lack of development with some alloys are still present and require more research.

Magnesium alloys are among the least developed alloys for the WAAM process, these alloys can provide a weight reduction of parts produced, which can lead to the reduction of emissions in the transportation sector.

This study aimed to successfully deposit the AZ61A Magnesium alloy using an in-house built GMAW-Based WAAM machine. By varying the parameters of the process, the Heat Input (HI) during deposition was affected and its impact on the material was studied.

During the project four walled-like samples were deposited, each with its own set of parameters and consequently heat input. First, the Wire Feed Speed (WFS) was established, and other parameters were iterated in accordance with deposition stability and weld bead appearance. The samples had significant internal defects and the process was characterized by deposition instability due to the process instability and material reactivity. The mean grain size was similar between the samples (17.49-22.93 μm). As expected from the similar grain size, microhardness was similar as well with a slight tendency to decrease as HI increased. Tensile testing was only conducted for sample S1 due to internal defects.

During this project, several obstacles such as, dissimilar materials, deposition instability, and thermal properties of the Magnesium alloy were detrimental to the successful deposition of samples. Acceptable parameters were obtained, and the resulting properties characterized. To further the application of these alloys in GMAW-Based WAAM, development is needed.

Keywords: WAAM, Magnesium, GMAW, Mechanical properties

RESUMO

A Manufatura Aditiva é considerada uma parte integrante da 4ª Revolução Industrial, permitindo avanços em cada etapa da produção. Nesta categoria, os processos de *Direct Energy Deposition* em específico, *Wire and Arc Additive Manufacturing* (WAAM) demonstram a capacidade de elevadas taxas de deposição, capacidade de produzir grandes peças. Contudo ainda são presentes defeitos, como poros e fissuras e a falta de desenvolvimento aplicado a outras ligas. As ligas de magnésio estão entre as ligas menos desenvolvidas para o processo WAAM, podem proporcionar uma redução de peso das peças produzidas, o que pode levar à redução das emissões no sector dos transportes.

Este estudo visou depositar amostras no formato de uma parede com a liga de Magnésio AZ61A, utilizando a máquina de WAAM desenvolvida no departamento com uso da tecnologia de soldadura GMAW. Ao se estabelecerem os parâmetros para a deposição das amostras houve uma variação da entrega térmica, a sua influência nas propriedades foi analisada.

Durante o projeto, foram depositadas quatro amostras. Primeiro, o *Wire Feed Speed* (WFS) foi estabelecido, os outros parâmetros foram iterados de acordo com a estabilidade de deposição e a aparência do cordão. As amostras tinham defeitos internos significativos e o processo foi caracterizado pela instabilidade de deposição e reatividade do material. O tamanho médio do grão foi semelhante entre as amostras (17,49-22,93 µm). A microdureza também foi semelhante, com uma ligeira tendência para diminuir à medida que a entrega térmica aumenta. Os ensaios de tração apenas foram realizados para uma amostra devido a defeitos internos. Durante este projeto, vários obstáculos como, materiais diferentes, instabilidades de deposição, e propriedades térmicas da liga de Magnésio, foram prejudiciais para o sucesso da deposição das amostras.

Foram obtidos parâmetros aceitáveis, e as propriedades resultantes foram caracterizadas. Para promover a aplicação destas ligas em WAAM com uso da tecnologia GMAW é necessário mais desenvolvimento.

Palavras chave: WAAM, Magnésio, GMAW, Propriedades mecânicas

CONTENTS

LIST OF FIGURES

List of Equations

List of Abbreviations and Symbols

AM	Additive Manufacturing
WAAM	Wire and Arc Additive Manufacturing
UTS	Ultimate Tensile Strength [MPa]
EL	Elongation [%]
RP	Rapid Prototyping
CAD	Computer-aided Design
SL	Stereolithography
DED	Direct Energy Deposition
PBF	Powder Bed Fusion
BJT	Binder Jetting
SLM	Selective Laser Melting
EBM	Electron Beam Melting
LMD	Laser Material Deposition
WLAM	Wire and Laser Additive Manufacturing
GTAW	Gas Tungsten Arc Welding
PAW	Plasma Arc Welding
BTF	Buy-to-Fly
MIG/MAG	Metal Inert/Active Gas

CMT	Cold Metal Transfer
WFS	Wire Feed Speed [m/min]
U	Voltage [V]
I	Current [A]
CTWD	Contact To Work Distance [mm]
TS	Travel Speed [mm/min]
GFR	Gas Flow Rate [l/min]
Tp	Pulse Time
Tb	Background Time
FGM	Functional Graded Materials
HCP	Hexagonal Close-Packed
HI	Heat Input [J/mm]
η	Efficiency
dV	Vickers Diagonal [µm]
BM	Base Material

1

INTRODUCTION

1.1 Motivation

As current societal demand shifts towards personalized and high geometry complexity parts, the industry must adapt and innovate, hence the application and development of AM over the last two decades. Environmental challenges, currently affecting the world, are also an important factor to consider, higher efficiencies in production stages are highly sought after.

While conventional manufacturing processes have been developed extensively, these are severely limited when considering the current demands with: longer times to manufacture, lower material usage efficiency, and incapable of producing high geometry complexity parts. AM can meet these demands with satisfactory results, mostly with metallic materials, and has gained significant attention of the Academia and Industry.

Conventional manufacturing, in contrast to AM, consists of a starting material that is subjected to successive subtractive processes, which is generally associated with poor material usage. AM consists of addition processes manufactured layer-by-layer. Most processes use a heat source and a filler material to add consecutive layers until the final part is achieved.

Amongst AM processes, the most common heat input is laser, however for WAAM, an electric arc is used, resembling conventional welding processes. Despite the first being the most used, electric arc is finding increasing applications due to its higher depositions, and ease of use, thus making it economically more advantageous.

1.2 Objectives

This project aims to study the production of magnesium alloy, AZ61A, using an automated arc welding process, WAAM, and the impact of the process and parameters on the

deposited layers on the final mechanical and structural properties. Specifically, the welding technology used will be Gas Metal Arc Welding.

The specific objectives are as follows.

- determine an acceptable set of process parameters for AZ61A magnesium alloy using GMAW;
- produce walled-like samples;
- characterize the samples in terms of mechanical and microstructural properties.

1.3 Document structure

This thesis consists of 5 chapters, each with its own sub-chapters.

Chapter 2 is the literature review of the thesis, it provides brief explanations of important aspects of Additive Manufacturing such as the different existing processes; welding technologies; important variables of WAAM, among others.

Chapter 3 presents how the work was conducted. Exhibits the materials and equipment used and the methodology behind the deposition and characterization of the samples produced, with schematic representations when necessary.

Chapter 4 encompasses the results and observations. Microscopies are presented along with the mechanical properties of the samples.

Chapter 5 summarizes the main conclusions of this work and presents a possible future work to advance this topic.

2

LITERATURE REVIEW

In this chapter, a brief overview of Additive Manufacturing (AM), current studies regarding the development of Wire and Arc Additive Manufacturing, and relevant studies regarding magnesium alloys are considered.

2.1 Additive Manufacturing

ASTM Standard F2792 - 12a, defines AM as a process of joining materials to make objects from 3D model data, usually layer upon layer, as opposed to subtractive manufacturing methodologies [1].

The term Rapid Prototyping (RP) is used in a variety of industries to describe a process for rapidly creating a system or part representation before final release. In other words, the emphasis is on creating something quickly, generally a basis model from which the final product will be derived. Over the last decades, due to innovations, parts produced using RP technology have become closer to the final part, and more importantly, functional, thus overcoming the label "prototype". AM is an RP technology where parts are produced using an additive approach [2].

It is a category of processes whereby parts or components are directly built from a solid model, a computer-aided design (CAD) file. The process involves slicing a solid model of the part into multiple layers, creating a toolpath to trace the individual layers; the part is then built layer by layer using a heat source and a filler material all of which are managed by a computer-controlled automated machine [3]. AM can be applied to a wide range of materials as listed: polymeric materials, composites, metals, and ceramics.

AM was first introduced in 1987 with the process stereolithography (SL) which is used for 3D systems [4]. Over the last two decades, AM has become increasingly important to many

industries, such as aerospace, automotive, and biomedical, as can be observed by the AM revenues for the end market in 2018, shown in Figure 2.1 [5].

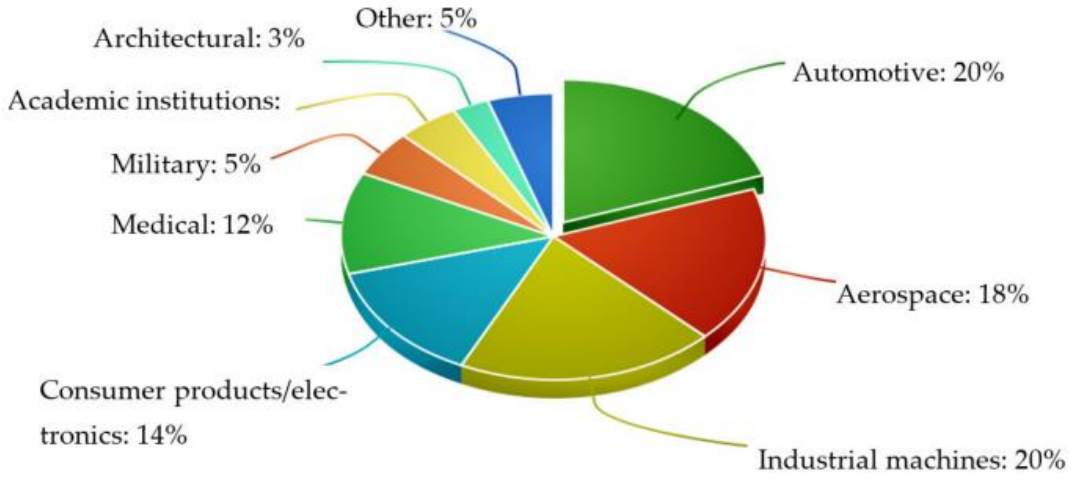

Figure 2.1 - Industrial adoption of AM [5].

During the last decades AM has been intensively developed, to standardize terminology of new technologies, ASTM created several categories of the fundamental functioning principles of current AM technologies. The seven main categories of AM processes and their definitions proposed by ASTM are the following [1].

- **Binder Jetting -** a liquid binding agent is selectively deposited to join powder particles;
- **Direct Energy Deposition (DED) -** material is deposited and melted via thermal energy onto a specified surface, where it solidifies;
- **Material Extrusion -** the material is drawn through a nozzle, where it is heated and is deposited layer by layer;
- **Material Jetting -** a printhead dispenses droplets of a photosensitive material that solidifies under ultraviolet light;
- **Powder Bed Fusion -** each powder bed layer is selectively fused by using an energy source like laser or electron beam;
- **Sheet Lamination -** sheets of ribbons of metal are bound together with the use of ultrasonic welding;
- **Photopolymerization -** an ultraviolet (UV) light is used to cure or harden a liquid photopolymer resin, whilst a platform moves the object being made downwards after each new layer is cured.

Compared to conventional manufacturing, each of these groups of processes are capable of manufacturing components with complex geometries. Conventional machining, such as forging, machining, and die casting are often impractical and have associated high costs and material waste. Some of the advantages associated with AM are presented in Table 2.1.

Table 2.1 - AM's technology opportunities. Adapted from [6].

Technological characteristics of AM - Opportunities
+ Direct digital manufacturing of 3D product designs without the need for tools or molds;
+ Increase in design complexity (e.g., lightweight designs or integrated cooling chambers);
+ High manufacturing flexibility: objects can be produced in any random order;
+ Allows for product design changes, without compromising the production line;
+ Production of functionally integrated designs in one-step;
+ Shorter lead times, lower inventories;
+ Less scrap and fewer raw materials required.

AM offers the capability of achieving high complexities and resolution, high material usage efficiency, and near net shape production leading to reduced lead times, and reduction of the conventional multi-stage processes. For cost-intensive materials (e.g., titanium or tungsten), AM can be the manufacturing process of choice [2], [7]. Despite all the developments made over the last two decades, there are still some key limitations regarding AM, presented in Table 2.2.

Table 2.2 - AM's technology limitations. Adapted from [6].

Technological characteristics of AM - Limitations
- Part size is limited by build space;
- Quality issues of produced parts compromise reproducibility;
- Skilled labor and strong experience needed;
- Final surface quality is generally poor, requiring postproduction processes;
- Most AM processes are characterized by low deposition rates;
- Intellectual property rights and warranty related limitations;
- Missing quality standards.

2.2 AM for metallic materials

Metal AM dates back to as early as 1920s with a patent by Baker which made use of an electric arc and metal electrode to form walled structures [3]. AM applied to metals has been intensively developed over the last decades. Currently, there are four main processes being used for metallic materials, which are shown in Table 2.3.

Table 2.3 - Four main categories of AM for metal. Adapted from [8].

Main Categories of AM for metallic materials	
Powder bed fusion (PBF)	• Selective Laser Melting (SLM) • Electron Beam Melting (EBM)
Direct energy deposition (DED)	• Laser / e-beam • Wire fed / Powder fed
Binder jetting (BJT)	• Infiltration • Consolidation
Sheet lamination	• Ultrasonic AM (UAM)

2.2.1 Powder bed fusion

PBF processes were among the first AM processes to be commercialized, in which powder particles are selectively fused together using one or more heat inputs like an electron beam or a laser, making up the part layer by layer. It's suitable for low-to-medium volume, geometrically complex parts and is still a popular choice currently, as of 2020, representing 54% of the metal AM market [5], [9].

For these processes, high-density energy heat sources like laser and electron beams are used. After the CAD file is processed, slices of the model are created and a toolpath is determined, the material in the form of powder is selectively fused to form a layer. Between the deposition of layers, the building platform is lowered, and powder leveled, repeating this process until the final part is completed. A schematic representation of the process is shown in Figure 2.2.

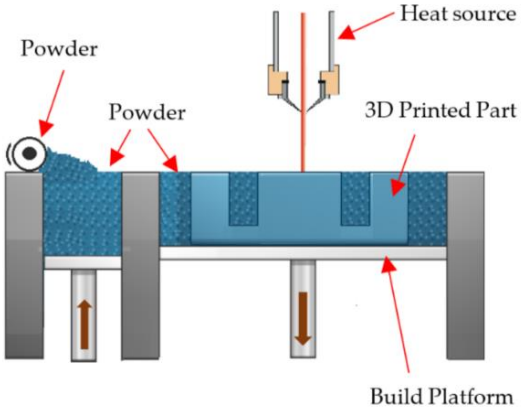

Figure 2.2 - Schematic representation of the powder bed fusion process [5].

EBM, performed in vacuum conditions, utilizes the kinetic energy of the electrons emitted to induce the powder particles into melting. It has limitations regarding materials, given that powder particles must be electrically conductive.

SLM, similar to EBM, is performed in a controlled environment, however, instead of using an electron beam, utilizes a high-power laser. The energy of the photons emitted is absorbed by the particles, thus increasing their temperature above the melting point.

PBF processes, despite being capable of manufacturing complex geometries with high accuracy present some limitations. Deposition rate is low (<0.2 kg/h) compared to WAAM (>3 kg/h), material used is highly processed and has a low utilization rate. All these limitations contribute to a higher manufacturing cost [8].

2.2.2 Binder Jetting

Binder Jetting processes are comprised of a metal powder bed similar to PBF processes, the binging of the particle is done through the use of liquid-state binder. Droplets of this binder are selectively dropped and cause the metal particles to aggregate, schematically represented in Figure 2.3.

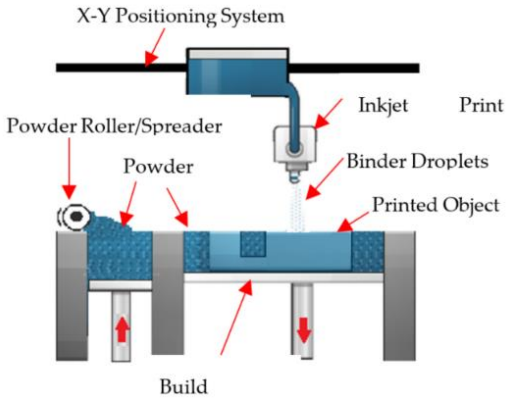

Figure 2.3 - Schematic representation of the binder jetting process [5].

This process is repeated layer by layer, each time the platform is lowered, and new powder placed over the previous layer using a roller/spreader.

This category of processes is characterized by being relatively quick and clean. However, its main drawback is the weak mechanical properties resulting from the process [5].

2.2.3 Direct energy deposition

Direct energy deposition processes are thermal energy focused, using an energy input. Feedstock material, powder, or wire is selectively melted and added onto the build platform. The most common energy inputs are laser beam, electron beam, plasma, or arc.

Currently, the three main processes in this category of AM are laser metal deposition (LMD), wire and laser additive manufacturing (WLAM), and wire and arc additive manufacturing (WAAM).

LMD, similar to SLM uses powder material, however the material is fed through the nozzle, reducing the setup preparation and space required, as shown in Figure 2.4. LMD is characterized by high efficiency and flexibility for manufacturing, which is beneficial to repair metallic components.

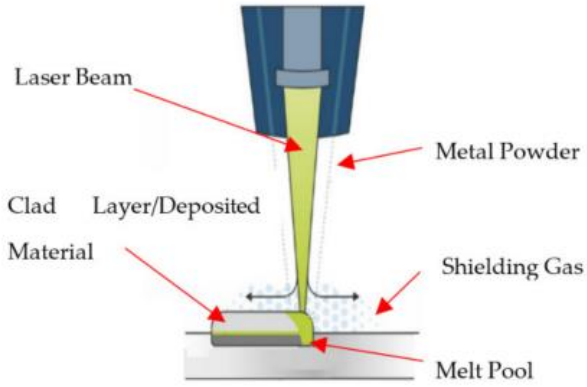

Figure 2.4 - Schematic representation LMD [5].

WLAM utilizes wire as feedstock and a laser beam as a heat source, shown in Figure 2.5. This system normally consists of a laser, an automatic wire-feed system, a computer numerically controlled worktable, or a robot system. The laser generates a melt pool on the substrate material, into which the wire is fed and melted, forming a bead. This process is compatible with several metals and alloys [10].

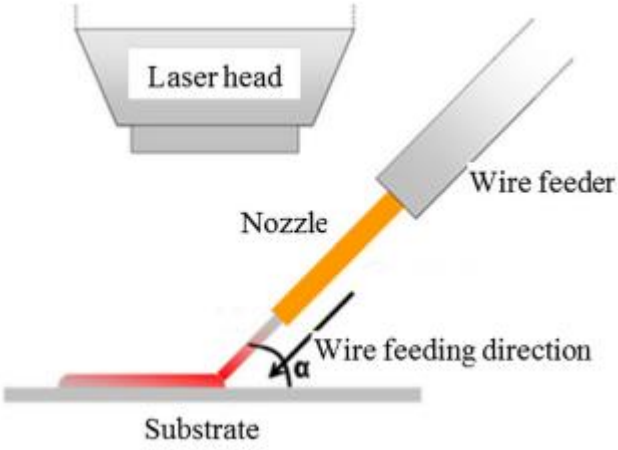

Figure 2.5 - Schematic representation WLAM [10].

Lastly, the process used for this project, WAAM represented in Figure 2.6, is defined as the combination of an electric arc used as heat source, and a wire as feedstock material. Capable of the highest material deposition rates of the DED category, WAAM can manufacture large and complex parts. Relies on the fundamental concepts of welding technologies that are largely mastered [11].

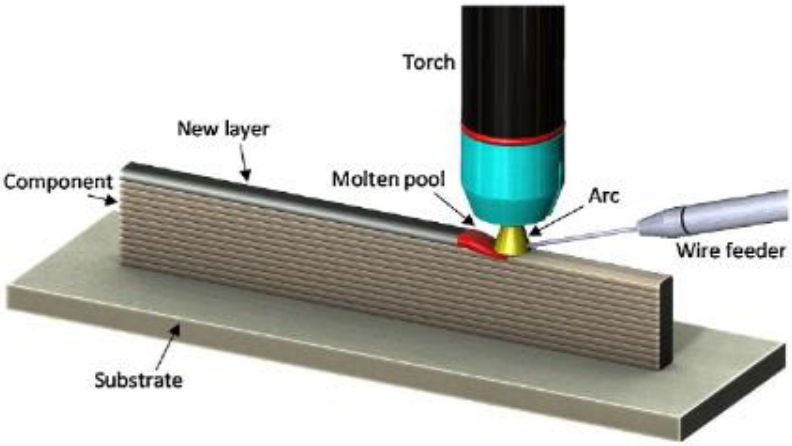

Figure 2.6 - Schematic representation WAAM [50].

2.3 Wire and arc additive manufacturing

WAAM relies on welding technologies that are largely mastered, the long research in arc welding for surfacing and joint welding, and the behavior of materials and processes behavior can be transferred [11].

Most metal AM systems have relatively low deposition rates and volumetric limitations, making them most suitable to manufacture small, complex components. Combining the

electric arc as the heat source, and wire as feedstock, the process is referred to as Wire and Arc Additive Manufacturing. It has introduced the possibility of higher deposition rates and increased working envelopes to produce parts, overcoming the limitations of other AM processes [9] like the low deposition rates of the PBF processes and others referred in Table 2.4 .

An example of WAAM applicability is shown in Figure 2.7, two different parts that have been tested for use in the industry. On the left, a ship propeller, and the right, a Pelton turbine.

Figure 2.7 - (Left) WAAM-manufactured propeller; (Right) WAAM-manufactured Pelton turbine blades [7].

Similar to other AM processes, WAAM has been shown to reduce fabrication time by 40-60% and post-machining time by 15-20%, compared to traditional manufacturing processes [9]. When compared to its popular AM equivalent, Laser-base powder AM, WAAM presents significant benefits, shown in Table 2.4.

Table 2.4 - Comparison between Laser-based powder AM and WAAM [8].

	Laser-based Powder AM	WAAM
Deposition rate	$0{,}1 - 0{,}2$ kg/h (low)	4 kg/h (high)
Utilization rate	$10 - 60\%$ (low)	$> 90\%$ (high)
Manufacturing cost	High	Low
Applicable workpiece	Complex, small workpieces	General, large workpieces
Manufacturing accuracy	$0{,}05$ mm (high)	$0{,}2$ mm (low)

As aforementioned, WAAM consists of welding technologies like Gas Metal Arc Welding, Gas Tungsten Arc Welding, and Plasma Arc Welding [12]. These welding processes are compatible with the same AM category, however, each of the processes have specific characteristics, advantages, and disadvantages. For this project, GMAW was chosen due to its versatility, deposition rates, and simplicity of use.

The application of these technologies has allowed for a near net shape production of components, reducing the need for posterior machining, which leads to the ability to

manufacture parts with a low Buy-to-Fly (BTF) ratio (ratio between the weight of the raw material purchased and the weight of the final part). For cost-intensive materials like titanium, a study was conducted, confirming that WAAM allowed for savings, which ranged from 7-69% while PBF processes proved to be more expensive than conventional machining [13].

2.3.1 Gas metal arc welding

GMAW, also known as metal inert gas (MIG) / metal active gas (MAG), is one of the most used welding processes in WAAM and has been used for many decades in surfacing, cladding, and AM. GMAW is a fusion-based arc welding process where the arc is established between the tip of a consumable wire and the workpiece under the protection of an inert or active shielding gas. When compared to the other two common welding processes previously mentioned, GMAW is capable of higher deposition rates thus making it ideal to produce large-scale parts [11].

This process uses an electric arc as a heat source, with the transmission of an electric current between a pair of conductors separated by gas, which ionizes. Unlike the GTAW or PAW processes, GMAW utilizes reverse polarity to take advantage of the heat generation in the electric arc, thus the consumable electrode (filler wire) is connected to the cathode (+) and the substrate is connected to the anode (-). Using this configuration, the cathode / filler wire is subjected to higher temperature within the electric arc due to the distribution of electrons and ions in the arc region. A schematic representation of the process is shown in Figure 2.8.

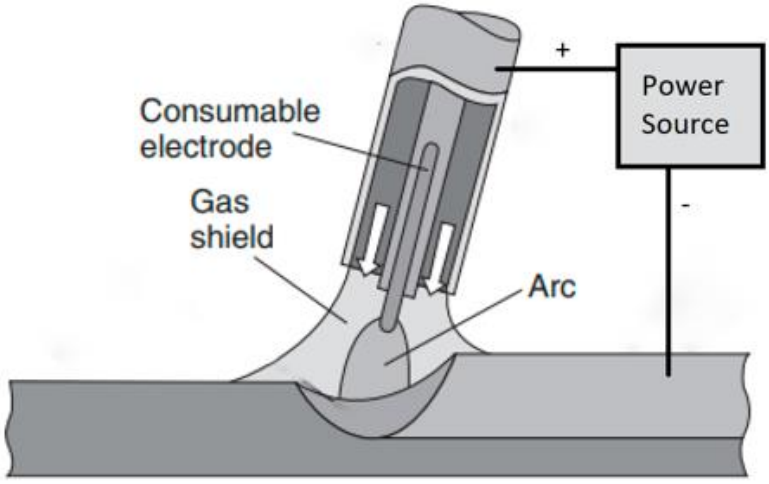

Figure 2.8 - Schematic representation of GMAW. Adapted from [14].

As MIG welding has a continuously fed wire process it is very easily mechanized. It has been applied to robotic welding in production lines due to its compatibility with almost any metallic alloy. Continuous welding, high deposition rates, and easily automated make GMAW an advantageous process to use for WAAM. The transition from GMAW to AM can be as simple

as coupling the welding equipment to a movement system with three or more axis, like a robotic arm.

While PAW is capable of achieving higher energy density which allows for faster travel speeds, and narrower beads, thus resulting in higher part accuracy, it also requires an increased investment due to the costly electric supply sources and the need for a rigid and precise feeding mechanism. Unless part accuracy is crucial, GTAW and GMAW processes are a more viable alternative, representing lower production costs.

Between GMAW and GTAW, the second still requires precise and more complex feeding mechanisms, representing higher costs, and a lower deposition rate. GMAW-based WAAM has higher deposition rates than the GTAW-based variant while also being more energy efficient [15], making it the most interesting alternative for industry applications. Due to the consumable electrode and its feeding system being coaxial to the welding torch, GMAW has an inherent simplicity of implementation and toolpath planning for AM [16].

Despite its benefits, GMAW presents negative aspects as well. Besides being characterized by deposition instability which leads to excessive spatter and internal defects it is also known for having a high energy density input [17]. This leads to an excessive heat input during the process, resulting in the creation of residual stress and geometric distortion of the final part [18]. To mitigate the issues related to the high thermal input, a modified GMAW process, cold metal transfer (CMT), was developed by Fronius. This variant provides a controlled method of material deposition and lower thermal input, leading to superior surface quality and a reduction of spatter during the process [19]. CMT has been successfully applied to additive manufacturing and more variants have been developed by Fronius, such as CMT pulse (CMT-P), and a CMT advanced (CMT-ADV) [11].

2.3.2 Process parameters

The main parameters of GMAW-based WAAM are the same as for GMAW, shown in Table 2.5.

Table 2.5 - Main parameters of GMAW.

Main process parameters of GMAW	
Wire feed speed (WFS)	[m/min]
Current intensity (I)	[amp]
Voltage (U)	[volt]
Contact to work distance (CTWD)	[mm]
Travel speed (TS)	[mm/min]
Wire diameter	[mm]
Gas flow rate (GFR)	[l/min]

According to a study conducted, after analyzing the width, height, and surface waviness, it was concluded that of the parameters above, GFR, WFS, TS, and voltage, were the most relevant, each affecting an aspect of the deposited layer. To influence the width, TS and WFS were the dominant parameters, for deposition rate WFS, and for surface waviness, TS presented the most influence in synergic pulsed welding mode [20].

For each material used in this process, a set of parameters will have a different outcome, and each time a new material is used there is the need to adjust and determine an ideal new set of parameters. The study has a comprehensive table directly linking parameters and their influence on the weld [20].

In GMAW there are four main transfer modes for the metal droplets which are mainly caused by the current and voltage used during the process; these are presented in Figure 2.9.

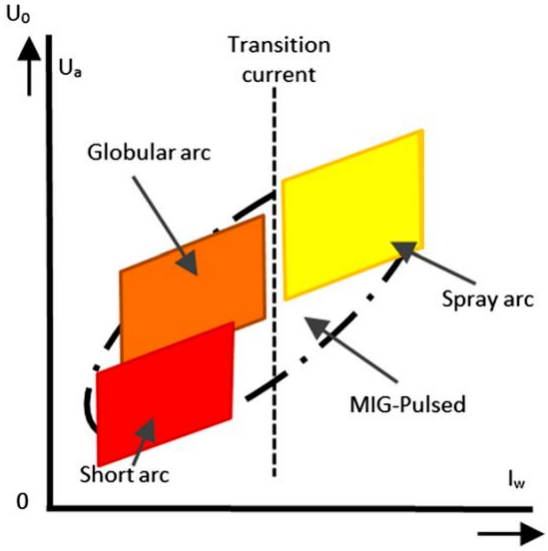

Figure 2.9 - Transfer modes according to arc current and voltage. Adapted from [21].

At lower voltages and lower intensities short-circuit mode happens. This mode has a lower heat input thus making it suitable for welding thinner parts. The stages are represented in Figure 2.10 and explained as follows: (A) arc ignites; (B) the electrode reaches the workpiece; (C) droplets are formed at the tip of the consumable electrode; (D) there is contact with the weld pool/workpiece; (D) due to the contact, a short-circuit occurs, extinguishing the arc; (E) droplets are pulled by the surface tension of the weld pool; (A) the arc can reignite again repeating this cycle [15].

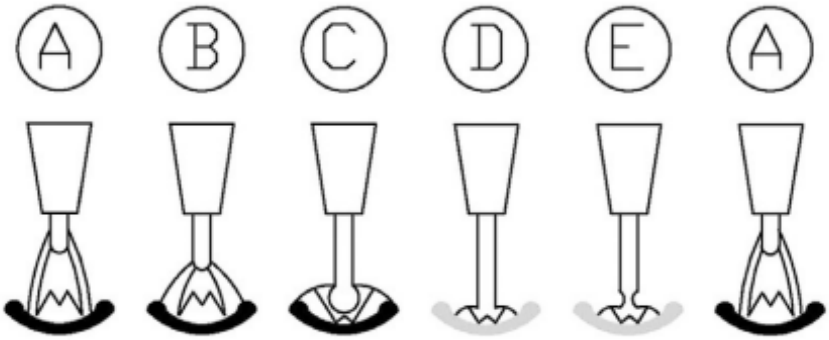

Figure 2.10 - Stages of short circuit transfer mode. Adapted from [15].

Globular transfer occurs at relatively low current intensity with all kinds of shielding gas. The droplets are generally larger than the consumable electrode's diameter, and irregular which leads to irregular weld beads, as represented in Figure 2.11. This transfer is the most undesirable of the four major GMAW transfer modes due to inconsistency, spatter, and instability [22].

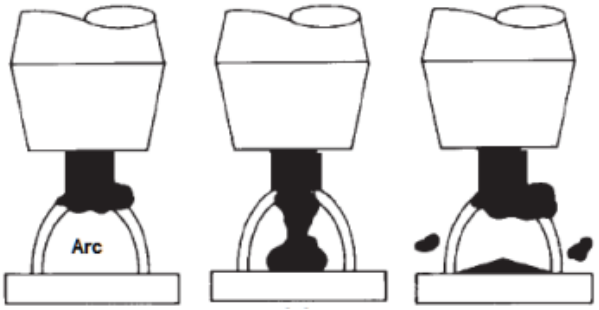

Figure 2.11 - Representation of globular transfer mode. Adapted from [22].

Spray and pulsed transfer modes take place past the transition current with the use of argon or argon-rich shielding gas. With spray transfer mode, small droplets are detached at a high frequency, guided by the electromagnetic forces due to the high currents, producing high-quality weld finish and high deposition rates. As for pulsed GMAW (P-GMAW), this mode aims to achieve the quality of the spray transfer mode with lower thermal input; other transfer modes are also obtainable while using P-GMAW [22]. P-GMAW spray is achieved by pulsing a current, which leads to lower average currents and as a result a lower heat/energy input, as shown in Figure 2.12.

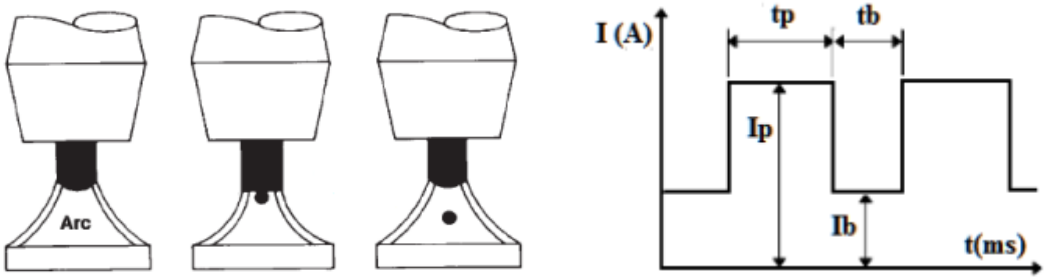

Figure 2.12 - Representation of the spray transfer mode; Current waveform: pulse time(tp); background time (tb); pulse current (Ip); background current (Ib) P-GMAW [22].

The shielding gas used in the welding process also has an important role in the transfer mode as well as the arc's characteristics. Its composition can influence the bead geometry, arc stability, weld appearance, and welding speed [23]. Each shielding gas has its own ionization potential, which is the energy expressed in electron volts required to remove an electron from a gas atom making it an ion, or an electrically charged gas atom.

Argon has a low ionization potential so its ionization can easily occur and has a better ignition which results in a more stable arc, for spray and P-GMAW, high concentrations of argon gases are used.

Another common inert gas is helium, which can be added to argon. It has a higher thermal conductivity that can increase the penetration and cooling rates of the weld pool. The other common gases, like CO_2 and oxygen are reactive gases. CO_2 can be used for MAG and

yields high travel speeds and deep penetration with low costs, however, using it solely also increases spatter formation and limits the transfer modes to globular or short-circuit.

2.3.3 WAAM process variants

For each layer deposited there is partial fusion of the metal base or previous layers deposited. When building fully dense parts this represents an obstacle due to the thermal gradient established which influences, for example, residual stresses and the final microstructure of the part. There have been recent developments from research groups that have given rise to new process variants to mitigate these disadvantages.

A variant that promotes plastic deformation of the layers was developed [24], consisting of a roller travelling over the deposited layers with a load of up to 100 kN, schematically represented in Figure 2.13.

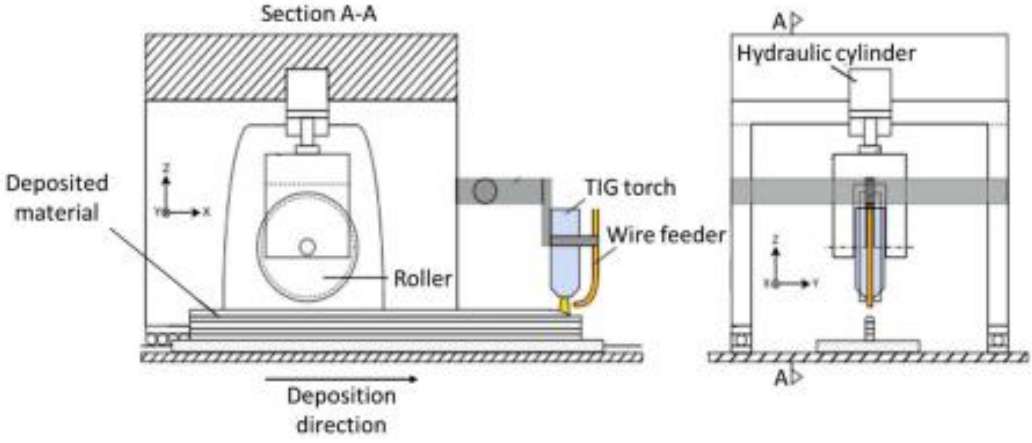

Figure 2.13 - Schematic representation of cold rolling WAAM process. Adapted from [24].

It was concluded that inter-layer rolling in WAAM of Ti-6Al-4V induced grain refinement, an overall modification of the microstructure from columnar grains to equiaxed grains. There have also been studies that combine inter-layer rolling with post heat treatment, which achieved higher mechanical properties such as ultimate tensile strength and elongation [25].

Another obstacle to the WAAM process is the porosity in the final parts, especially for Al and Mg alloys, thus compromising the mechanical properties. The formation of pores occurs mainly in aluminum and magnesium alloys, because when the material is melted its hydrogen solubility is higher than in its solid-state, so as the material cools and solidifies hydrogen is rejected and tends to form pores. Applying external forces to the layers can also contribute to the collapse, reduction of pore size, and decrease in pore quantity [11].

Besides using a roller to apply a load, machine hammer peening has also been studied and led to the enhancement of the final mechanical properties [26].

At higher temperatures, another process is hot forging WAAM (HF-WAAM), is a variant that consists of applying a load to the deposited material while it is in the viscoplastic region to reduce residual stresses, increase ductility, and homogenize grain structure [27].

There are other WAAM variants that do not rely on plastic deformation, such as active inter-layer cooling or heating. To control thermal cycles, a study used compressed CO_2 gas to actively cool the deposited layers; this led to better surface finish, refined microstructure and improved mechanical properties [28].

There are other variants that aim to introduce multiple wire feeding systems, shown in Figure 2.14, in order to increase deposition rates and manufacture functional graded materials (FGM) which are heterogeneous materials [11].

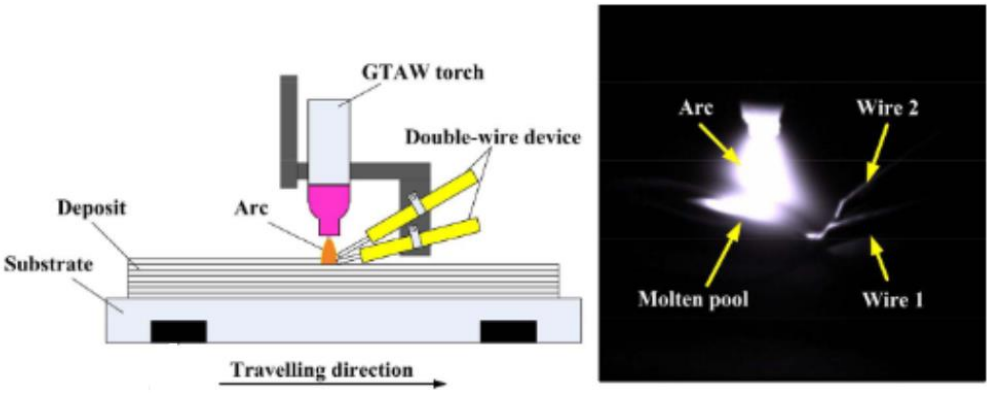

Figure 2.14 - Schematic representation of multiple wire WAAM variant [29].

In summary, due to the interdisciplinarity of the WAAM process, there are several possible routes for optimization of the process. To control and mitigate the negative aspects of the process while adapting it to the industry, enhanced solutions are necessary.

2.3.4 Path planning

In AM, path planning is an important factor to ensure both time and resource efficiency. A common problem with path planning occurs on each deposited layer; that is to say that at the start, with the ignition of the arc and low temperature of the substrate/previous layers, weld penetration is reduced while, at the end of the layer, low heat dissipation and continuous heat input leads to high temperatures, as shown in Figure 2.15, thus resulting in a wider bead with deeper penetration, reducing the layer height.

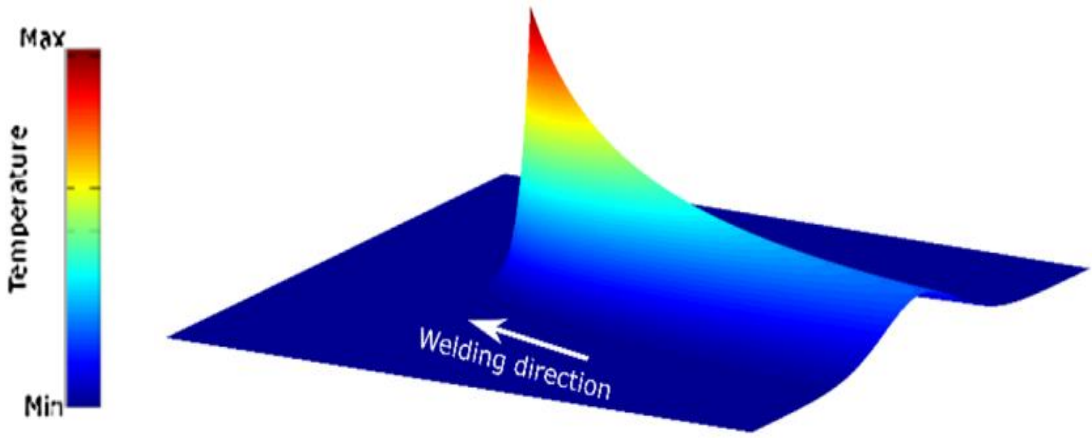

Figure 2.15 - Schematic representation of temperature evolution along the material for a welded joint. Adapted from [30].

Depositing consecutive layers in the same welding direction as the previous ones will lead to an accumulation of height differences along the bead. This problem can be solved by decreasing the TS and the current at the initial stage of the weld pass and increasing it at the end, as shown in Figure 2.16.

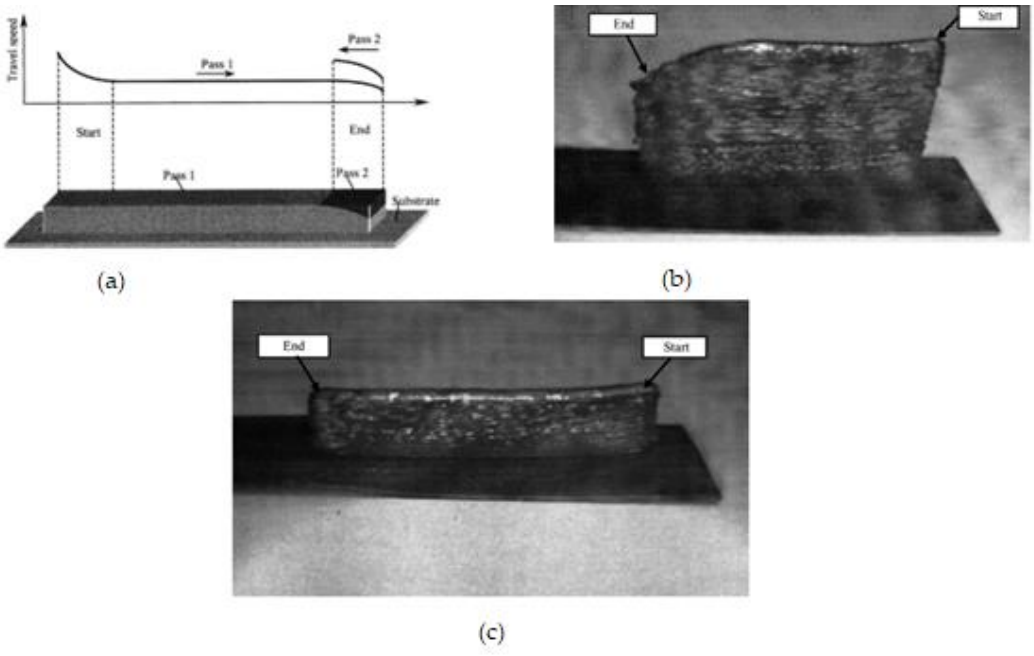

Figure 2.16 - TS control method (a); default deposition (b); controlled deposition (c). Adapted from [31].

It is also possible to mitigate this problem using a zig-zag approach, by switching the welding direction after each layer is deposited, leading to a more uniform layer. However, this will promote the formation of more heat affected zones due to the thermal accumulation which results in higher residual stress at the boundaries of the walls [32].

2.4 Materials

The base material and conventionally manufactured components will have different properties than additively manufactured components [33]. To ensure the final part quality, mechanical properties and microstructure, there is a need to understand the dependencies between the process variables and resulting material properties.

Additively manufactured components, specifically manufactured with the WAAM process, are subjected to repeated thermal cycles and, along with the problems mentioned above, this becomes problematic as each material can respond differently [33]. Thermal conditions like cooling/heating, path planning, and parameters must be set while taking the material's characteristics into account.

The thermal gradient is established along the deposited layers, normal to the substrate. While the material is cooling, the formation of grains will mainly occur along the gradient resulting in unwanted columnar grain structure [34]. This type of grain growth results in an anisotropic behavior which could be unwanted for multi-axial loading conditions. These grains are more susceptible to solidification cracking than equiaxed grains, which can better deform to accommodate contraction stresses, and having greater grain boundary area can positively influence mechanical properties [35].

WAAM is suitable for a wide range of materials, however the most used materials are steel, titanium, aluminum, and nickel-based alloys. Several alloys like Ti-based and Ni-based are increasingly being studied due to their inherent cost and possible applications. Following the adoption by the aerospace industry and the benefits of the process, the desire to mature this process has shown that the adoption of this process is increasing [11]. Some examples of what alloys are currently being used in the two main industries are shown in Table 2.6.

Table 2.6 - Application of alloys using WAAM in major industries. Adapted from [36].

Industries	Alloys				
	Ti-based	Al-based	Steel-based	Ni-based	Bimetal
Aerospace	x	x		x	x
Automotive		x	x		x

2.4.1 Magnesium alloys

Due to its strength-to-weight ratio, magnesium alloys are a promising alternative to aluminum for lightweight design, which, as previously mentioned, can represent a reduction of emissions and an overall increase of transportation efficiency. Mg alloys also have other interesting properties such as good mechanical damping, electromagnetic shielding, good machinability, recyclability and biodegradability.

Characterized by a hexagonal close-packed (HCP) crystal structure which, at room temperature represents few slip systems resulting in a poor formability. Plastic deformation is usually associated with defects and obstacles, however its formability can be enhanced through grain refinement and texture control with new processes [37]. Most Mg alloys are processed via die-casting and sand casting, the second being important for aerospace applications [38].

Despite its advantages and potential, due to its chemical reactivity, specifically the risk of ignition and flammability risk, its development has been hampered when compared to other alloys. With the addition of rare earth elements like zirconium and others, these risks are mitigated [39].

For production using the WAAM process, there are some examples of GTAW for AZ80M and AZ31 magnesium alloys with success [40], [41], GMAW for AZ31B [42], and the GMAW variant CMT [43]. Some key parameters are listed in Table 2.7.

Table 2.7 - Summary of key parameters used in other studies.

Alloy	Process	Current [A]	Voltage [V]	WFS [m/min]	Travel Speed [mm/min]	Ref.
AZ80M	GTAW	$I_{peak;base}$ 120;75	N.A.	1.15	300	[40]
AZ31	GTAW	$I_{peak;base}$ 136;91	N.A.	2	200	[41]
AZ31B	GMAW	$I_{average}$ 100	10	N.A.	800	[42]
AZ61A	CMT	$I_{average}$ 43	12.6	1.8	270	[43]

2.4.1.1 Microstructure and defects

WAAM is characterized by repeated depositions until the final part is achieved, layer-by-layer. This repetition represents thermal cycles and consequently establishes a thermal gradient perpendicular to the deposition plane throughout the part which influences the formation of the grain as the material solidifies. Despite not being a defect, the common resulting grain is columnar due to the thermal gradient, this grain results in a decrease of mechanical

properties and anisotropy when compared to conventionally manufactured parts. To control the formation of grain and improve these properties there is a need to control the final microstructure of the material and obtain a more desirable grain, equiaxed grains, which ultimately reduces crack susceptibility while improving other mechanical properties [11].

A study that aimed at refining the resulting grain of the process, GTAW-based WAAM, has achieved beneficial results using a Mg alloy (AZ31). By varying the pulse frequency, it was observed that a frequency between 5-10 Hz produced samples with smaller and more refined grains, as shown in Figure 2.17 [41].

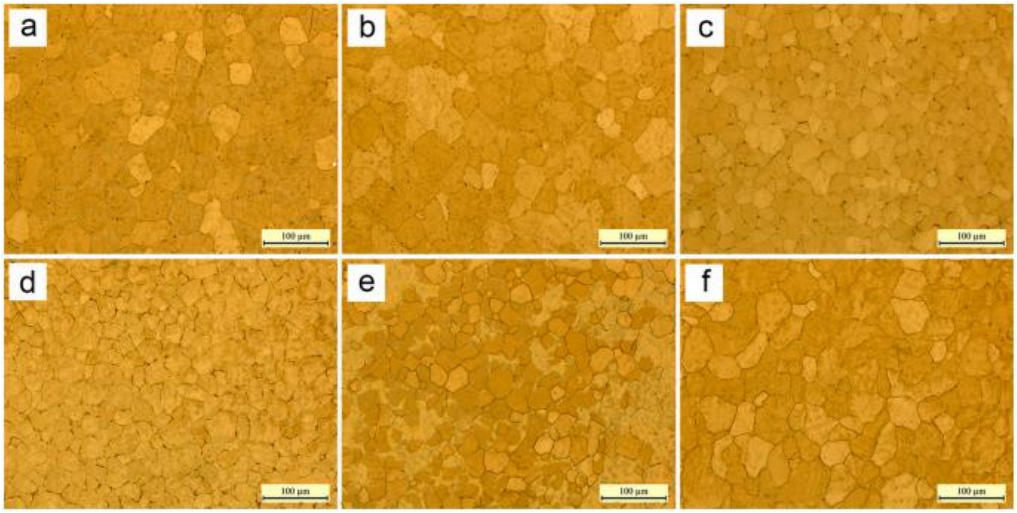

Figure 2.17 - Microstructures of the samples deposited by different pulse frequencies: (a) 500 Hz; (b) 100 Hz; (c) 10 Hz; (e) 5 Hz; (e) 2 Hz and (f) 1 Hz [41].

Grains deposited with a pulse frequency of 5 and 10 Hz showed the best results. At those frequencies, weld pool resonation was achieved which promoted oscillations of the pool decreasing cooling rates consequently. This grain refinement, caused by the weld pool oscillations also led to a poor geometry accuracy. With the refinement of the grain, there was an increase of mechanical properties.

Other methods to control the final microstructure include the addition of inoculant particles between the deposition of material. These particles are of other materials, generally with higher melting points than the filler material, and serve as a nucleation point for the formation of grains, promoting a more equiaxed formation during the solidification of the layer. This method is yet to be studied for Magnesium alloy.

3

EXPERIMENTAL PROCEDURE

This chapter contains all the information regarding the equipment, welding consumables and materials used during this project. The experimental approach and characterization techniques are presented next.

3.1 Materials

The material used as substrate was a structural steel plate, mild steel, with 70x250x8 mm dimensions. The consumable electrode or filler metal was a solid wire of AZ61A alloy with 1.6 mm diameter, from Dratec, the chemical composition is shown in Table 3.1.

Table 3.1 - Chemical composition of the alloy (weight %), AZ61A.

Material	Mg	Al	Zn	Mn	Si	Cu	Ni	Fe
AZ61A	92	5.8-7.2	0.4-1.5	0.15	0.10	0.05	0.005	0.005

The shield gas used was commercial pure argon; its composition is described in Table 3.2.

Table 3.2 - Composition of the shielding gas.

Material	Ar	H2O	O2	CO2
Alphagaz 1	99.999 %	<3 ppm	<2 ppm	<0.5 ppm

3.2 Equipment

In the following sub-chapters, the equipment that was used is listed and brief explanations of its operations are provided.

3.2.1 Welding equipment

The wire control unit used was a *Pro Mig 501* and the power source was a *Pro MIG 3200*, both models, shown in Figure 3.1, were manufactured by *KEMPPI*. These models are connected to the motion equipment and can be controlled remotely.

Figure 3.1 - Welding equipment.

This welding equipment has 3 MIG welding modes, each characterized differently: synergic pulsed wave, synergic continuous wave, and conventional continuous wave. Synergic welding modes only allow the selection of WFS, while current and voltage can be slightly adjusted using a trim/offset, and for a specified filler material and diameter, current and voltage are automatically adjusted. The conventional continuous wave mode allows to independently control the voltage and WFS values, the current is automatically determined.

Due to the chemical reactivity of magnesium alloys, synergic pulsed wave mode was used to attempt to mitigate the spatter, weld defects and reduce energy input. This welding mode is explained in detail in 2.3.2. The welding equipment used requires the user to define the material of the electrode, it does not have magnesium alloys as an option. Due to the similarities between magnesium and aluminum alloys, the equipment was set to weld aluminum alloys. This of course presents another degree of uncertainty for this parametrization.

3.2.2 Motion system

The system used was developed in [17], shown in Figure 3.2. The system has 3-axis which allow for three degrees of freedom. This system is controlled using the *Repetier Host* software which uses G-Code.

Figure 3.2 - Motion system 3 axis [17].

.

3.2.3 Deposition strategy

As previously mentioned in Chapter 2, the deposition strategy is relevant to the thermal gradient and consistency of the deposited layers. Due to the high thermal conductivity of magnesium alloys and lower melting point of magnesium alloys, a zig-zag approach to the deposition was chosen when possible, to mitigate the inconsistencies at the start and end of each weld bead, as schematically represented in Figure 3.3. Due to difficulties associated with the instability of the process and consequent ramping, height differences along the wall prevented this strategy from being used.

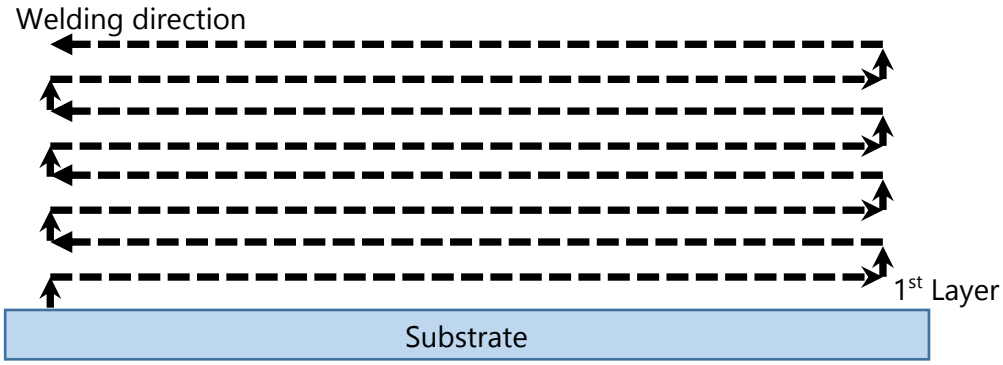

Figure 3.3 - Schematic representation of the deposition strategy.

3.3 Heat input

Due to their reactivity and lower fusion points, magnesium alloys are susceptible to evaporation during the welding process. To mitigate vaporization, spatter and porosity, the CMT process is generally used given that it is capable of achieving lower energy inputs.

Each set of parameters used to produce walled-like samples has its own heat/energy input, which can be calculated according to (3.1).

$$HI = \frac{U \cdot I}{TS} \cdot \eta \quad \text{[J/mm]} \qquad (3.1)$$

The values used for the voltage and current intensity were the means measured by the welding equipment during the process. The efficiency, η, considered for the process was 0.7 according to [44].

3.4 Characterization techniques

The approach used to determine deposition and characterization parameters/methods is explained in the following sub-chapters.

3.4.1 Deposition and preparation of samples

Due to the lack of literature regarding the application of magnesium alloys with GMAW technology, an extensive iterative process took place until acceptable parameters for deposition were achieved.

Four samples were manufactured with characteristic sets of parameters. For each of the samples, a WFS was set for the welding equipment while TS, CTWD, and trim values were tested and chosen out of a domain of values. The approach used to establish the four sets of parameters, is schematically represented in Figure 3.4.

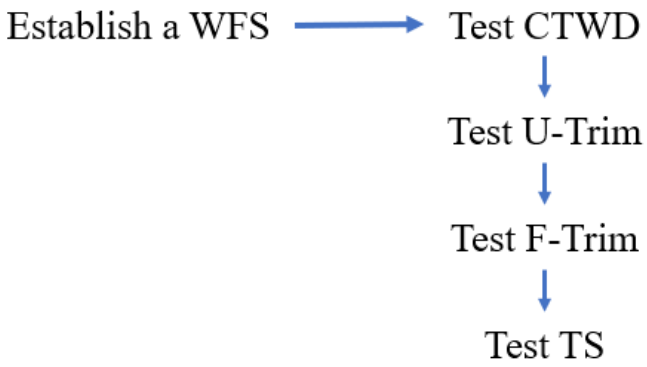

Figure 3.4 - Schematic representation of deposition approach.

As stated above in Chapter 2.3.2, for P-GMAW the parameters with the most influence are WFS and TS, while the remaining have a smaller impact on the final weld bead.

The main parameter in this process is WFS. It is established first, given that it is responsible for the deposition rate. This allows for an optimization of the remaining parameters. Each parameter, in the order represented in Figure 3.4 was tested with at least four different values.

In this example, the WFS was set to 3 m/min and TS set to 450 mm/min. CTWD is established secondly, this was observed to have the most influence on the stability of the arc; several values were tested as represented in Table 3.3.

Table 3.3 - Parameter method - CTWD tests.

Weld bead image	Test Nº	CTWD [mm]
	P1	11
	P2	13
	P3	15
	P4	17

As seen in Table 3.3, P1 through P3 show an inconsistent weld bead with lack of deposited material along the bead. This is due to the poor arc stability throughout the deposition which resulted in unstable arc formations, promoting excessive spatter. Test P4, out of the four tests conducted, has the most uniform weld bead, so the CTWD for the following stages was set to 17 mm.

U-Trim, responsible for controlling arc length in the welding mode, was determined next; four values were tested while maintaining the other variables constant. WFS set to 3 m/min; CTWD set to 17 mm.

Table 3.4 - Parameter method - U-Trim tests.

Weld bead image	Test Nº	U-Trim
	P4	0
	P5	-1
	P6	-2
	P7	-3
	P8	-4

From Table 3.4, test P6 has a noticeable gap of deposited material. This was caused by the adjustments made by the synergic welding mode, with the first arc ignition the power source automatically adjusts the parameters, however, these are often detrimental to the rest of the weld bead and require more time to stabilize. From the tests conducted, P8 had the most stable arc and uniform weld bead, therefore the voltage trim was set to -4 for the remaining tests. This increase in stability and uniform weld bead is due to the arc length, with the decrease in offset of the voltage its length is decreased and thus decreasing the distance that the droplets of molten material must travel to reach the substrate, leading to a more precise placement of material.

The same process was repeated adjusting the F-Trim which is responsible for offsetting the welding dynamics. Welding dynamics can be referred to as the rate of rise of the current,

this ultimately influences the temperature of the process and frequency. By adjusting it positively, there is a higher rate of current rise leading to a cooler and narrower bead, while adjusting it negatively slows the rate of rise of current, making the process hotter and promoting the weald bead to be wider. Varying the values from 2 to -2, the best weld bead was chosen to set the parameter, F-Trim was set to -2. Finally, applying the same method as explained previously the TS was determined.

Between depositions, each steel substrate used was prepared, using an angle grinder, and cleaned with acetone. The deposited wall samples were easily detached from the steel substrate due to the dissimilarities between the two materials. Steel and magnesium are non-reactive and non-mutually soluble [45].

3.4.2 Optical microscopy

To prepare the samples for microscopy and microhardness measurements, slices were cut, roughly 20 mm after the start of the weld bead in order to avoid the arc ignition area, as shown in Figure 3.5, (a), and then put in a mold with resin, (b).

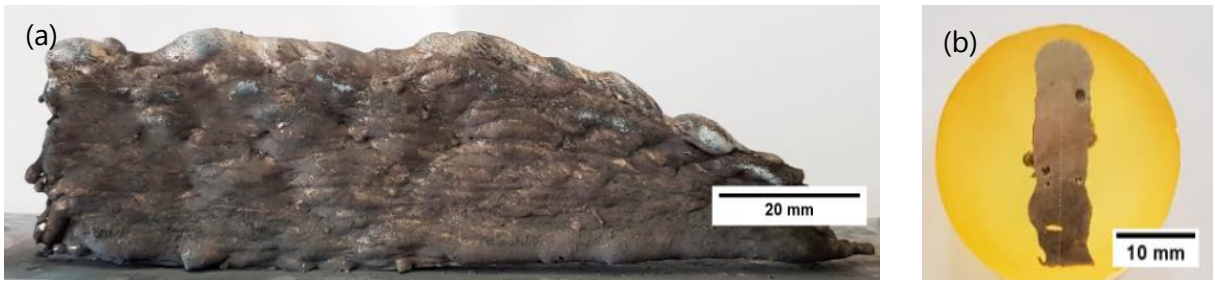

Figure 3.5 - Schematic representation of the preparation of samples for microscopy; (a) slice used; (b) sample in resin.

To observe the samples, the samples in resin were polished using silicon carbide paper from 80 to 1000 grit size (P80 - P2500) and then polished again with an abrasive alumina paste with 1 μm.

The samples were then etched, immersed with gentle agitation for roughly 20 seconds using the following solution: 5 mL of acetic acid; 10 mL of water; 6 g of picric acid; 100 mL of ethanol (95%).

To examine and register the microstructures of the samples, the equipment used was Olympus CX40.

3.4.3 Vickers microhardness testing

After completing the microscopy analysis and etching, the samples in resin were used for Vickers microhardness testing. The microhardness was measured using *Mitutoyo HM-112*, following the vertical line along the wall represented in Figure 3.6, using a load of 1 kgf ($HV_{1.0}$) and a dwell time of 10 seconds.

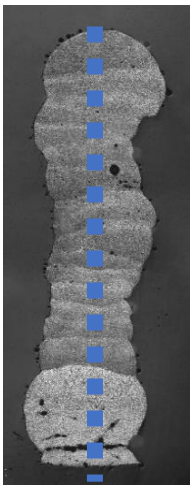

Figure 3.6 - Schematic representation of the micro-vickers indentations.

The distance between indentations was determined in accordance with [46], the minimum distance was calculated the following Equation (3.2).

$$D = 2{,}5 \cdot \mathrm{dV} \quad [\mu m] \qquad (3.2)$$

For the first indentations, the average dV was approximately 170 µm which meant the minimum distance required was 425 µm, the distance used was 450 µm.

3.4.4 Uniaxial tensile test

To prepare the specimens for the uniaxial tensile test, the deposited walls were firstly machined at a horizontal milling machine, manufactured by *Henrique Holke, model F-1010*, to flatten and reduce the thickness of the wall to 2mm, Figure 3.7.

Figure 3.7 - Machined deposited wall.

After machining the walls, a 3D model of the wall was created and the designed specimens for the tensile test were outlined to create the file required to machine them at the CNC Machine, *Super Mini Mill 2*, manufactured by *HAAS*. To fixate the machined walls in the machine, each wall was screwed on the ends to a piece of aluminum. Final product is shown in **Erro! A origem da referência não foi encontrada.**.

Figure 3.8 - Tensile Specimen.

The uniaxial tensile tests were then performed at room temperature, at CENIMAT, on a *Shimadzu* tensile machine. Due to internal defects in the deposited walls, this test was only possible for one of the four walls.

4

RESULTS AND DISCUSSION

In this chapter, a brief overview of the parameters is presented followed by the results and characterization of the samples manufactured. In the end, there is a discussion regarding these results.

4.1 Parameters and samples

As previously described, the method to determine acceptable process parameters was conducted each time WFS was changed. Each deposited sample consisted of 30-60 layers of deposited material. The sets of parameters used are described in Table 4.1.

Table 4.1 - Parameters of manufactured samples.

Sample	WFS [m/min]	TS [mm/min]	CTWD [mm]	U-Trim	F-Trim	SGR [l/min]	Nº Layers
S1	3	500	17	-4	-1	19	31
S2	3.5	500	12	-5	0	19	56
S3	4	550	14	-4	0	19	39
S4	5.5	700	19	-1	0	19	36

Due to several variables, like dissimilar materials, electrode extensions with some wear and technical difficulties associated with the motion system, obstacles like ramping and collapse of the end of the walls during the deposition could not be easily addressed. This led to the impossibility of depositing the same number of layers for each sample, the samples frequently detached from the substrate or ramping caused significant height differences. Interlayer temperature was 40º Celsius between depositions.

The energy input, as previously mentioned, can influence the microstructure, and promote the vaporization of Mg in the deposited material, which ultimately can alter its mechanical properties. In Table 4.2, relevant values used to calculate the energy input are listed along

with the estimated energy input throughout the deposition of a single layer according to each set of parameters.

Table 4.2 - Heat inputs per sample.

Sample	U_a [V]	I_a [A]	TS [mm/min]	WFS [m/min]	HI [J/mm]
S1	21.4	38	500	3.0	68.31
S2	23.2	46	500	3.5	89.64
S3	24.3	60	550	4.0	111.34
S4	22.8	94	700	5.5	128.58

4.2 Microstructure

The final microstructure of the deposited samples is of great importance, it will have a significant influence on the other properties of the samples. The overall transversal view of the wall of sample S1 is represented in Figure 4.1

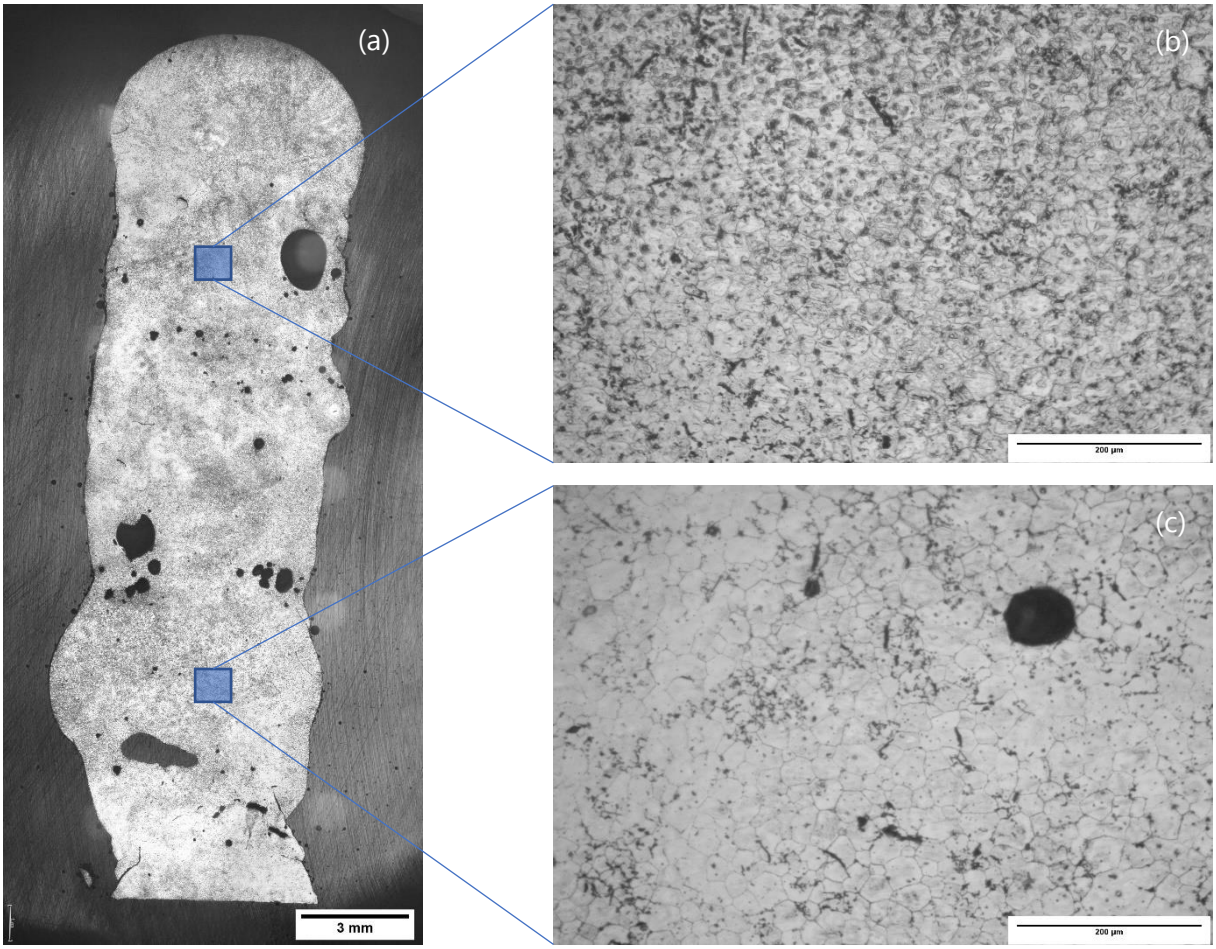

Figure 4.1- Microscopy of S1; (a) transversal view, 2x magnification. Scale bar 3mm; (b) 20x upper zone; (c) 20x bottom zone. Scale bar 200 µm.

In Figure 4.1, (b) and (c) the grain boundaries are visible. The upper part of the sample (b) was overexposed to the etching solution, thus creating darker spots that are corroded pits. This could have been mitigated by shortening the etching period or diluting the solution used. With 20x magnification, the grain boundaries are visible as well as pores and fissures. From the literature provided, Mg alloys mostly tend to form small, equiaxed grains and this is confirmed for all the samples.

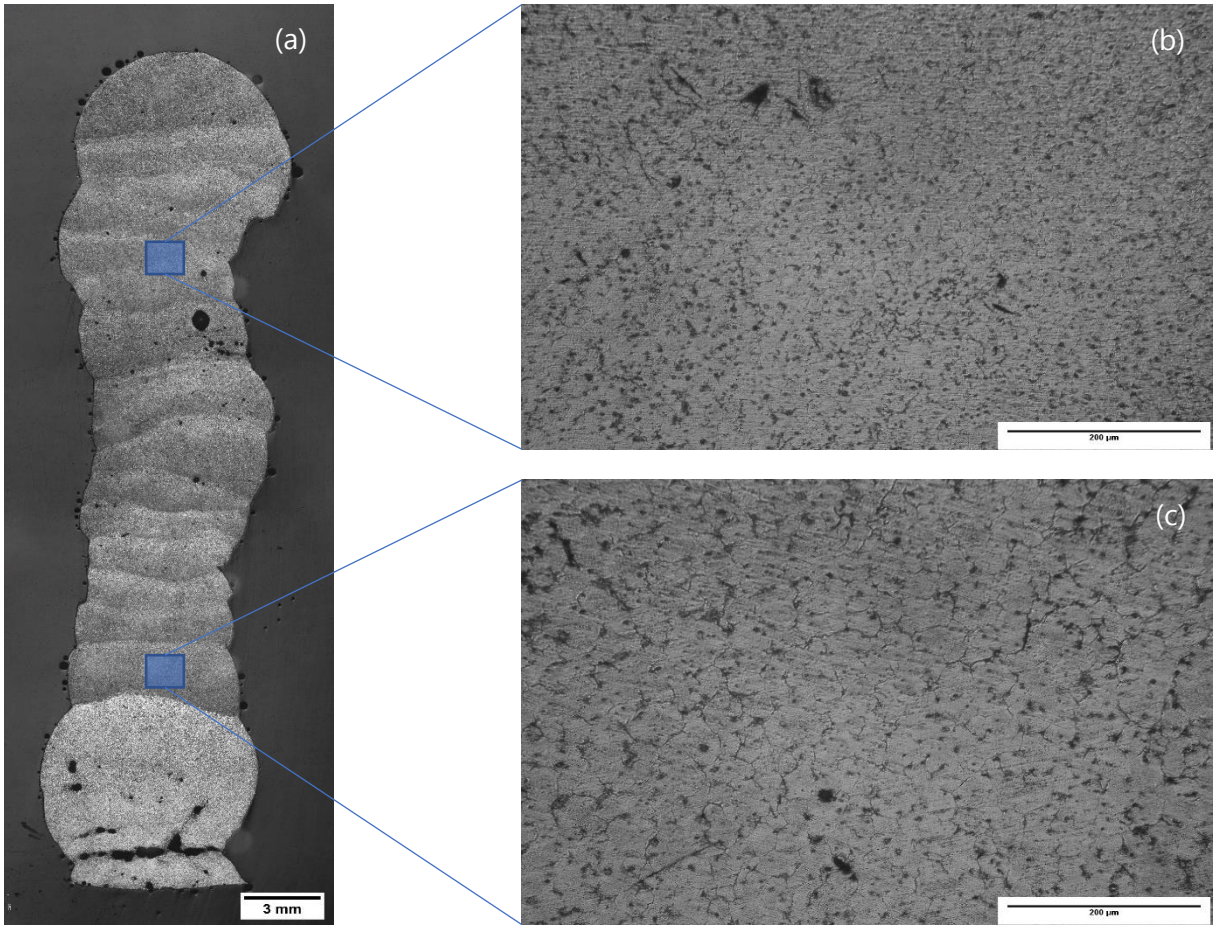

Figure 4.2 - Microscopy of S2; (a) transversal view, 2x magnification. Scale bar 3mm; (b) 20x upper zone; (c) 20x bottom zone. Scale bar 200 µm.

The interface between adjacent layers, in Figure 4.2, can be observed throughout the height of the deposited wall of sample S2, at the bottom part, there is no separation due to the re-melting of the previous layers, resulting in a seemingly homogenous layer. There are several pores, a significant concentration near the substrate-layer interface.

Represented in Figure 4.3, is the observed microstructure of sample S3.

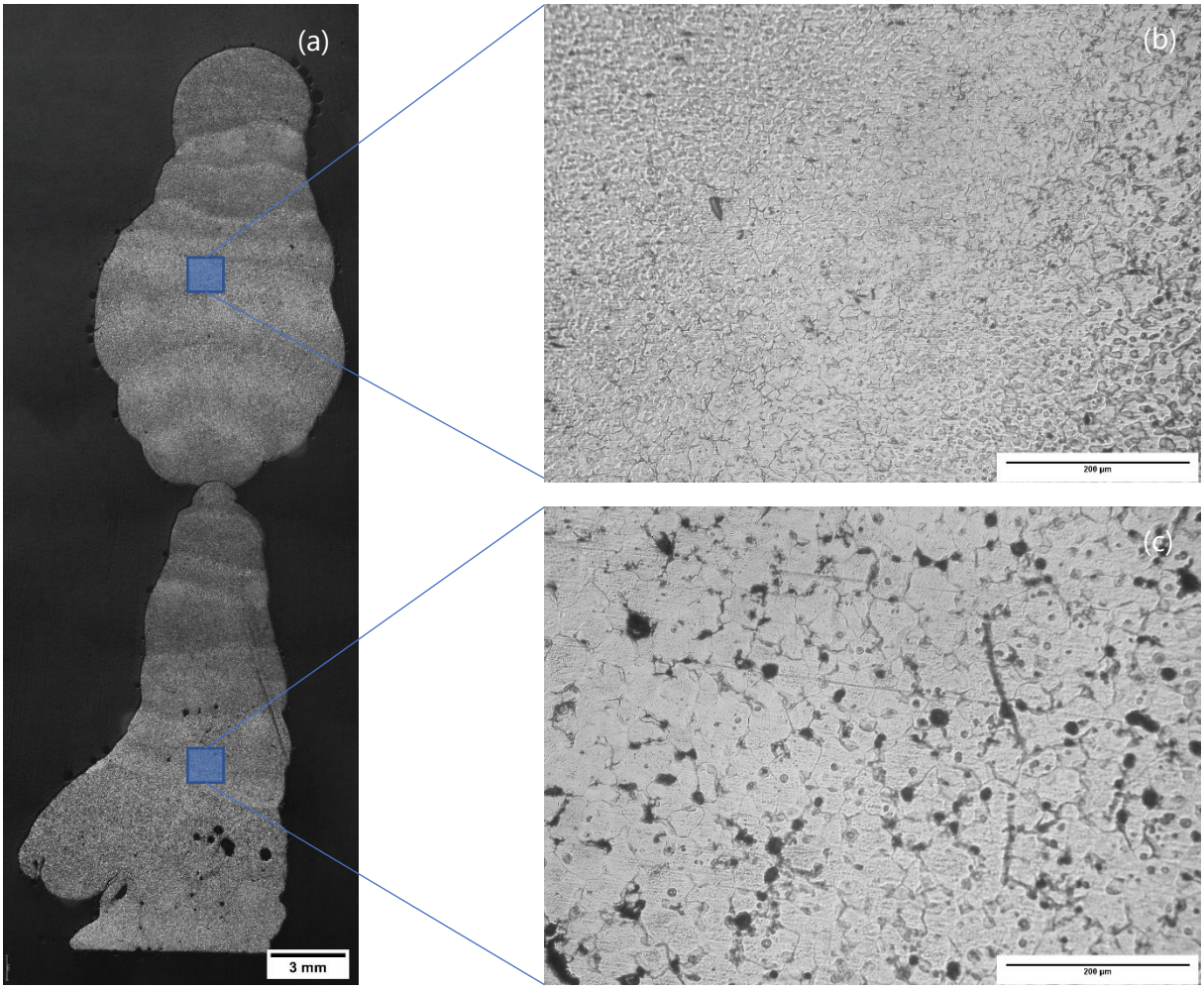

Figure 4.3 - Microscopy of S3; (a) transversal view, 2x magnification. Scale bar 3mm; (b) 20x upper zone; (c) 20x bottom zone. Scale bar 200 µm.

Pores can be observed in (a) as well as the interface between adjacent layers. In (b), Figure 4.3, the grain boundaries are not as clear as in (c), this is a result of the different cooling rates along the wall, leading to different concentrations of phases and composition in each zone, these phases react differently to the etching solution used. This could have been mitigated by using a different etching solution.

As seen in Figure 4.4, sample S4 has higher pore concentration. This can be related to the higher energy input out of the four sets of parameters. Small cracks and pores can be easily identified in (a), Figure 4.4.

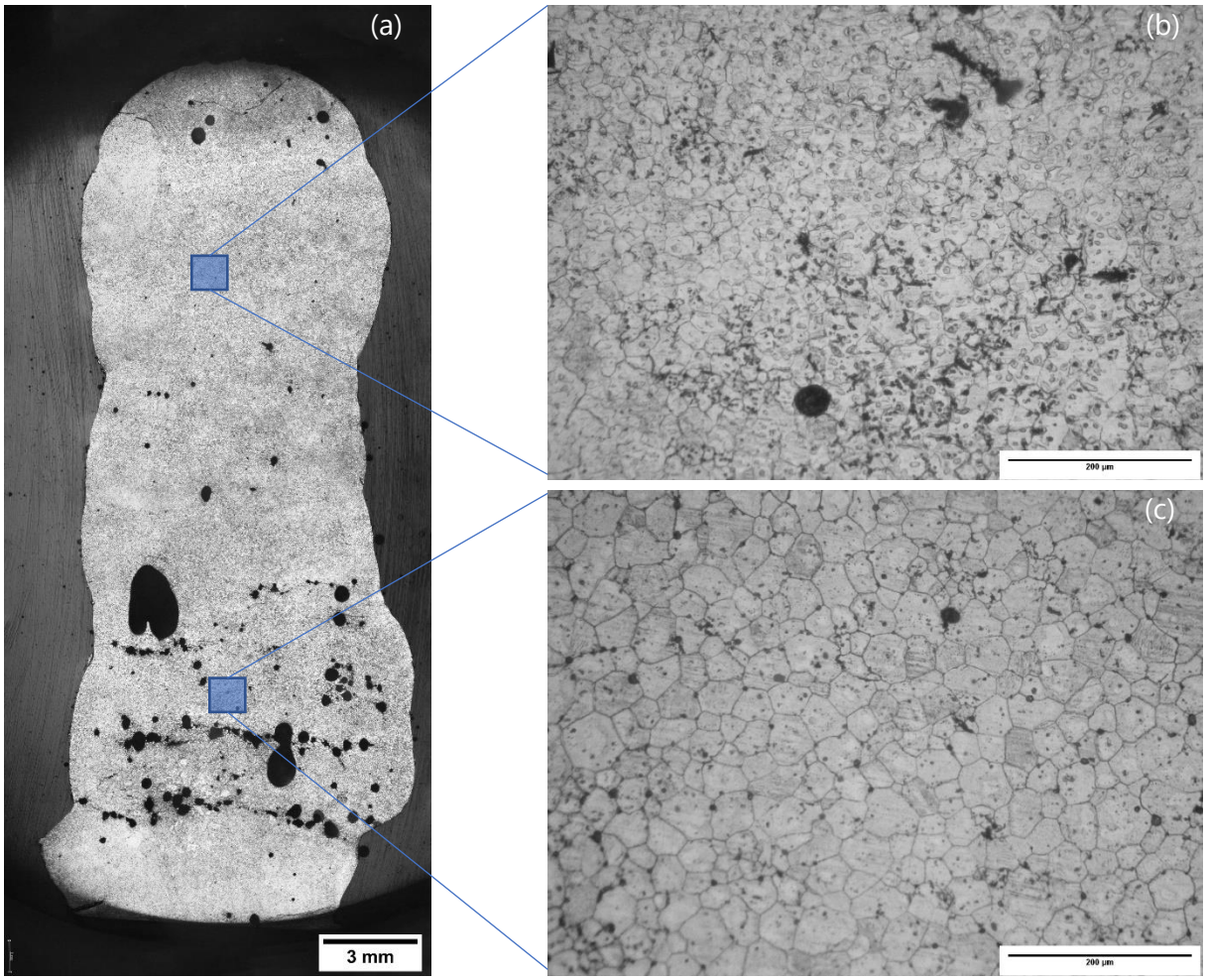

Figure 4.4 - Microscopy of S4; (a) transversal view, 2x magnification. Scale bar 3mm; (b) 20x upper zone; (c) 20x bottom zone. Scale bar 200 µm.

The pores visible in all the samples can be categorized into two. Smaller dispersed pores can be linked to gas porosity, caused by humidity, entrapment of protective gas and the decrease of solubility of hydrogen as the material solidifies, while the larger pores are caused by arc instability, inclusion of impurities, agglomeration of gas porosity, and vaporization of alloy elements.

4.2.1 Grain characterization

To measure the grain size and the grain aspect ratio, using the software *ImageJ*, the line intercept method was used, as depicted in Figure 4.5.

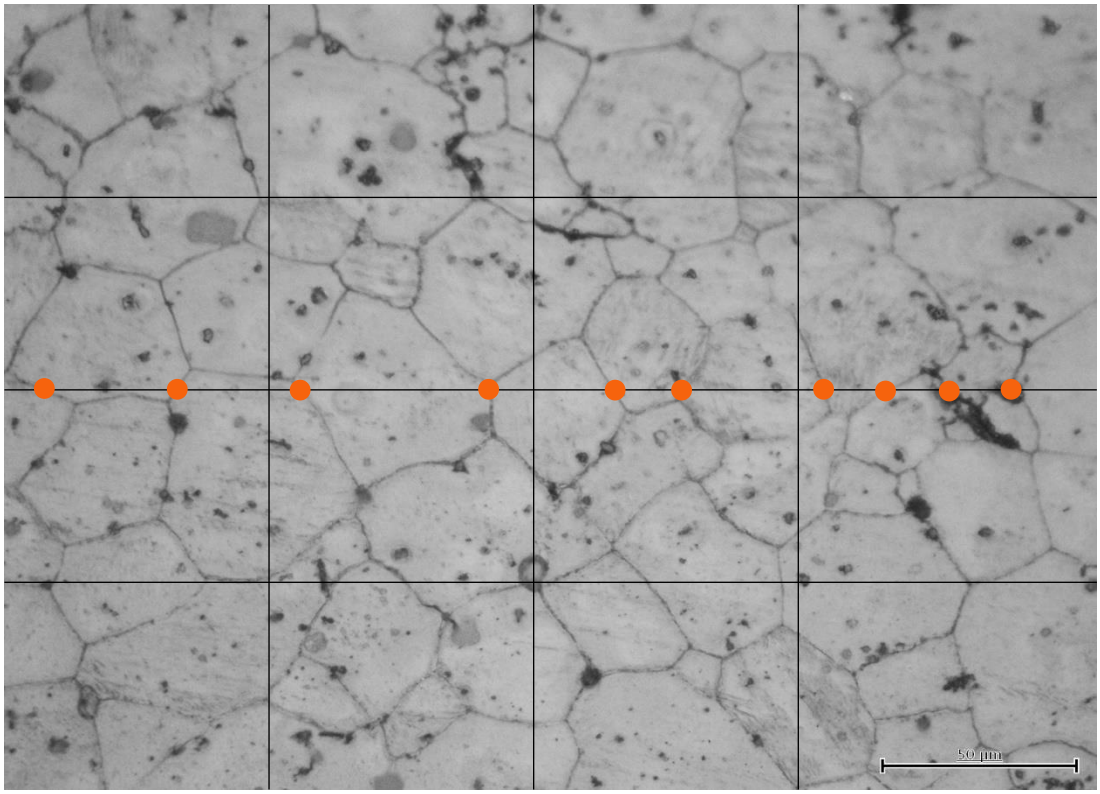

Figure 4.5 - Schematic representation of the intercept method (50x magnification S4).

The method used was: three lines are plotted with the same distance between them, both vertically and horizontally; the interceptions, when test lines intersect grain boundaries, are counted with specific values (1 for tangential intersections, 0.5 when the end of the test line ends on a grain boundary, 1.5 when the test line intersects a triple point); lastly, by using Equation (4.1), the average grain size is calculated. The aspect ratio is analyzed by comparing the grain sizes along the horizontal and vertical orientation, which could have an influence on anisotropy behavior.

$$d = \frac{l}{N} \qquad (4.1)$$

To facilitate the counting of the intersections, a x50 magnification was used. This allowed for a clearer perspective of the grain boundaries. An example of the intercept method is represented in Figure 4.5, the image is a 50x magnification of sample S4.

The orange dots represent the interceptions of the middle test line with the grain boundaries. The middle test line has a length of 278.00 μm and there are nine regular intersections and one triple point intersection. Using (4.1), the average grain size calculated is 26.47 μm. This method was repeated for the three horizontal and vertical test lines.

In Table 4.3, the grain sizes and grain aspect ratios of the samples are presented.

Table 4.3 - Grain size and aspect ratio.

Sample	Grain size (μm)	Grain Aspect Ratio (V/H)	Heat Input [J/mm]
S1	17.49 ± 1.74	0.94	68.31
S2	16.57 ± 3.24	0.96	89.64
S3	19.51 ± 5.13	1.12	111.34
S4	22.93 ± 4.75	0.93	128.58

The studied literature regarding AZ61A alloy has achieved similar results, 21-39 μm [41], 31 ± 12 μm [47], and 27 μm [43].

The grain aspect ratio allows for an easier interpretation of the differences in grain size between the vertical and horizontal direction, all the samples except S3 have an aspect ratio inferior to 1. Due to the proximity of these values to 1, it can be assumed that the deposited material will have a near to anisotropic response, this will be evaluated in the tensile testing.

4.3 Vickers microhardness

The hardness of the samples has a direct link to the microstructure and the remaining mechanical properties. The average hardness of each sample is presented in Table 4.4 while the following figure, Figure 4.6, shows the evolution of the hardness along the height of the wall for each sample.

Table 4.4 - Mean hardness of samples.

Sample	Vickers microhardness ($HV_{1.0}$)	Heat Input [J/mm]
S1	60.9 ± 3.4	68.31
S2	61.1 ± 2.9	89.64
S3	61.0 ± 4.3	111.34
S4	58.0 ± 2.4	128.58

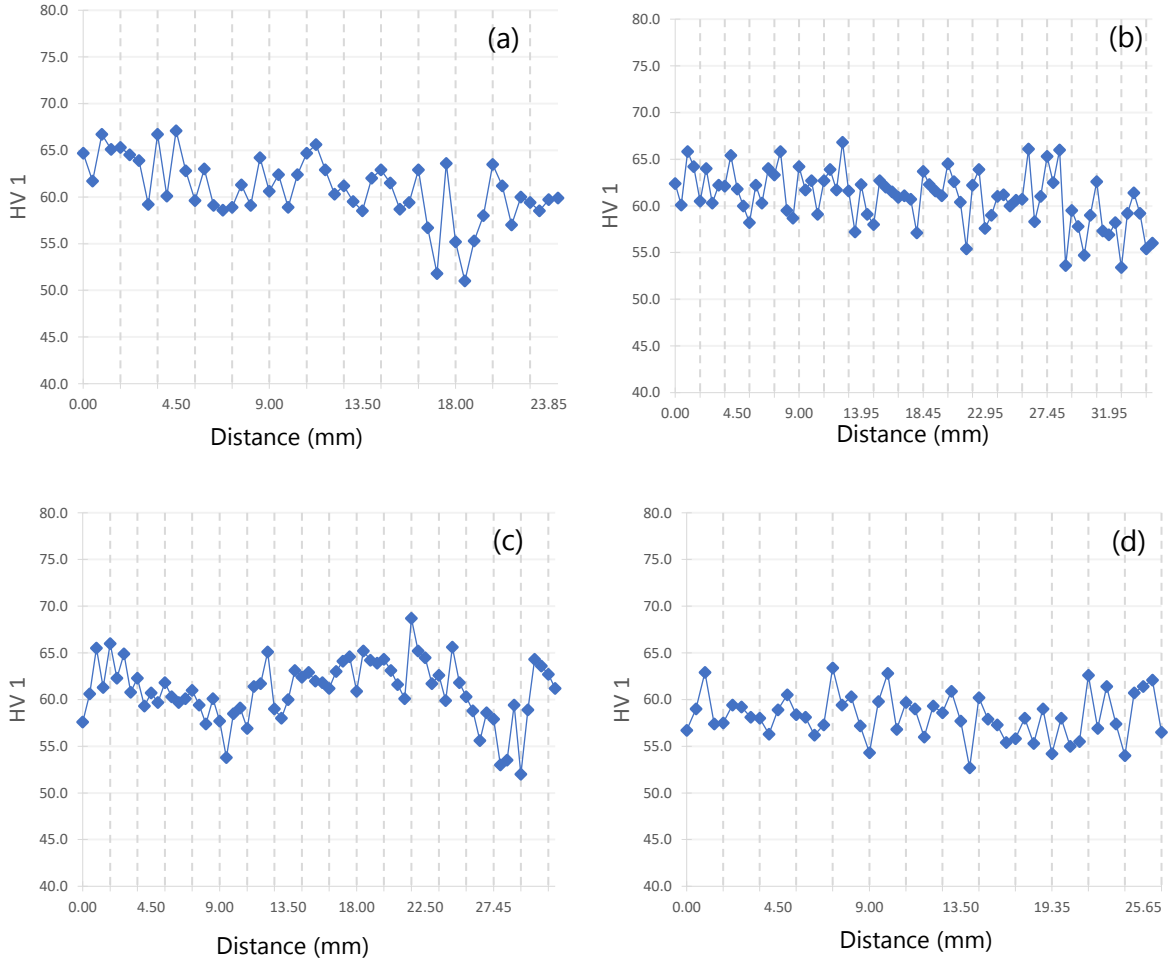

Figure 4.6 - Micro-Vickers hardness distribution; (a) Sample S1; (b) Sample S2; (c) Sample S3; (d) Sample S4.

Microstructure and hardness values are directly linked, since the values for the grain size of each sample are similar, the hardness values of these samples were also expected to be similar. However, a tendency was noted, with the increase of HI the microhardness showed a slight decrease.

Higher hardness values, at the top and bottom of the samples, was expected due to the higher cooling rates at the substrate interface and lack of intrinsic heat treatment at the top layer; however, it was not observed. This can be explained by the lack of fusion and adherence of the magnesium to the steel substrate which results in lower cooling rates than expected, and at the top this can be explained due to the influence of the interlayer temperatures still being high.

4.4 Tensile properties

Tensile tests were conducted for two specimens in both directions of the deposited wall, sample S1. The base material (BM), or filler metal, was also tested. Results are presented in Table 4.5.

Table 4.5 - Tensile properties.

Sample	UTS (MPa)	EL (%)
BM	262	10.95
Horizontal	193 ± 2	6.16 ± 0.47
Vertical	188 ± 4	5.39 ± 0.65

Yield strength could not be calculated due to the internal defects of the specimens, the evolution of tension was not as uniform as expected. As expected, the response from the material was similar for both directions of load, another indicative of anisotropic behavior.

Table 4.6 - Tensile properties from literature.

Direction	UTS (MPa)	EL (%)	Ref.
Vertical	256 ± 10	15.3 ± 3.5	[43]
Horizontal	264 ± 2	15.4 ± 0.7	
N.A.	221 - 263	23 - 27.3	[48]
Vertical	272 ± 4	17.2 ± 1.3	[47]
Horizontal	275 ± 1	16.8 ± 0.4	

The results from the revised literature, in Table 4.6, show that the obtained results are lower than expected. Elongation values and tensile properties are significantly lower due to the inability to control and mitigate the defects like porosity and hot cracking, observed in Figure 4.4.

4.5 X-ray diffraction analysis

For each sample, an x-ray diffraction analysis was conducted. To analyze the results, the software *DataViewer* by *PANalytical* was used. The peaks registered correspond to the α phase, comprised of Mg, and the β phase, made of $Mg_{17}Al_{12}$.

In Figure 4.7, the combined diffractograms are shown and it is visible that these do not present significant differences in peak intensity or angles, which means there was no significant change in terms of phase formation throughout the samples. Some of the peaks are identified, given that the angles are the same, the observed phases should be the same [49].

From this diffractogram it can be inferred that the range of HI tested did not promote the formation of different phases on each sample.

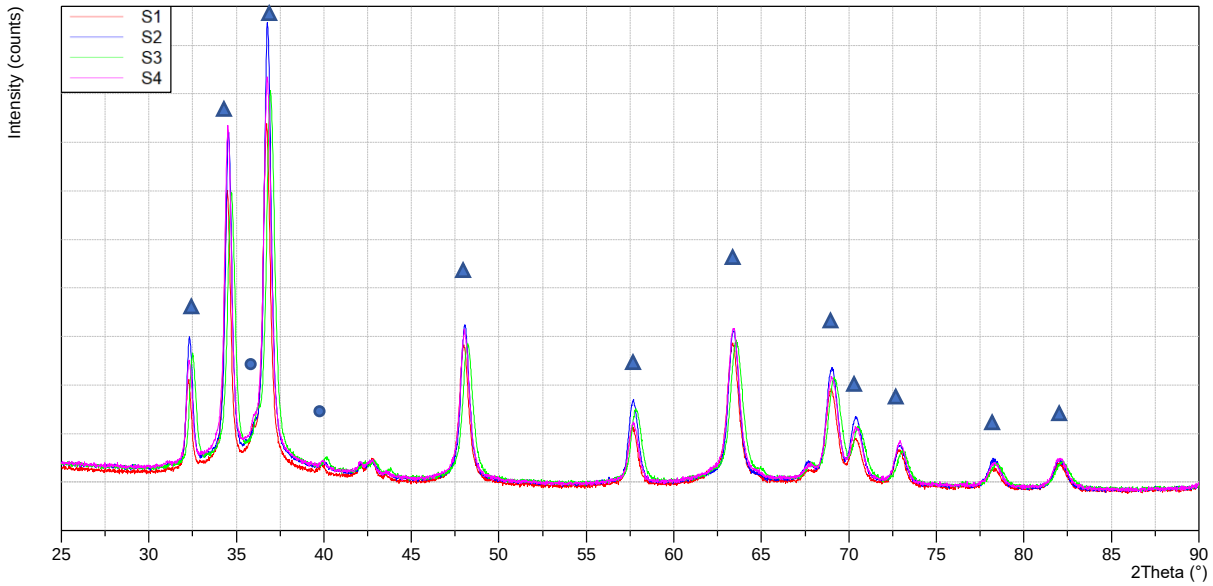

Figure 4.7 - Combined XRD diffractograms of the samples. ▲ - Mg; ● - $Mg_{17}Al_{12}$

5

CONCLUSIONS AND FUTURE WORK

The application of AZ61A Mg alloy with GMAW-based WAAM was achieved with reasonable results during this study. Four sets of parameters were tested, and samples characterized. With this study some key aspects can be concluded:

- Magnesium alloys still lack development with GMAW welding technology, there are many difficulties associated that are not yet fully understood;
- As energy input increases, so does porosity. This can be caused by an increase in arc instability and burn-off alloy elements vaporization;
- Mechanical properties were not optimal due to internal defects, such as pores and cracks. Other processes with a better control of energy input and more stable deposition, such as CMT and TIG, have achieved better results;
- Despite lower mechanical properties, the hardness and grain size achieved was in-line with the results from the revised literature;
- From the grain aspect ratio and tensile properties, it can be concluded that samples produced using this process have a nearly anisotropic behavior;

Despite not achieving optimal parameters or results, due to the potential of light metals such as Mg alloys, this study provides an entry point for other studies regarding GMAW-based WAAM for such alloys. There are clear obstacles stated that require a deeper understanding. Therefore, to allow for wider use of Mg alloys in the WAAM category, the specific areas that require more research and future work are:

- Methodical approach to parameter optimization;
- Chemical composition of the produced samples using this process, to provide a better understanding of the effects of alloy elements vaporization, such as magnesium;
- Deeper mechanical characterization, specifically tensile testing of different samples.

BIBLIOGRAPHY

[1] ASTM F2792-12a, "Standard Terminology for Additive Manufacturing Technologies," *ASTM International*, 2012, doi: 10.1520/F2792-12A.

[2] I. Gibson, D. W. Rosen, and B. Stucker, "Introduction and Basic Principles," in *Additive Manufacturing Technologies: Rapid Prototyping to Direct Digital Manufacturing*, I. Gibson, D. W. Rosen, and B. Stucker, Eds. Boston, MA: Springer US, 2010, pp. 20–35. doi: 10.1007/978-1-4419-1120-9_1.

[3] B. Dutta, S. Babu, and B. Jared, "Chapter 1 - Metal additive manufacturing," in *Science, Technology and Applications of Metals in Additive Manufacturing*, B. Dutta, S. Babu, and B. Jared, Eds. Elsevier, 2019, pp. 1–10. doi: https://doi.org/10.1016/B978-0-12-816634-5.00001-7.

[4] S. R. Singh and P. Khanna, "Wire arc additive manufacturing (WAAM): A new process to shape engineering materials," *Mater Today Proc*, vol. 44, pp. 118–128, 2021, doi: https://doi.org/10.1016/j.matpr.2020.08.030.

[5] A. Vafadar, F. Guzzomi, A. Rassau, and K. Hayward, "Advances in Metal Additive Manufacturing: A Review of Common Processes, Industrial Applications, and Current Challenges," *Applied Sciences*, vol. 11, no. 3, 2021, doi: 10.3390/app11031213.

[6] C. Weller, R. Kleer, and F. T. Piller, "Economic implications of 3D printing: Market structure models in light of additive manufacturing revisited," *Int J Prod Econ*, vol. 164, pp. 43–56, 2015, doi: https://doi.org/10.1016/j.ijpe.2015.02.020.

[7] K. Treutler and V. Wesling, "The Current State of Research of Wire Arc Additive Manufacturing (WAAM): A Review," *Applied Sciences*, vol. 11, no. 18, 2021, doi: 10.3390/app11188619.

[8] J. Liu, Y. Xu, Y. Ge, Z. Hou, and S. Chen, "Wire and arc additive manufacturing of metal components: a review of recent research developments," *The International Journal of Advanced Manufacturing Technology*, vol. 111, no. 1, pp. 149–198, 2020, doi: 10.1007/s00170-020-05966-8.

[9] I. Gibson, D. Rosen, B. Stucker, and A. Khorasani, *Additive Manufacturing Technologies*. 2020. doi: 10.1007/978-3-030-56127-7.

[10] D. Ding, Z. Pan, D. Cuiuri, and H. Li, "Wire-feed additive manufacturing of metal components: technologies, developments and future interests," *The International Journal of Advanced Manufacturing Technology*, vol. 81, no. 1, pp. 465–481, 2015, doi: 10.1007/s00170-015-7077-3.

[11] T. A. Rodrigues, V. Duarte, R. M. Miranda, T. G. Santos, and J. P. Oliveira, "Current Status and Perspectives on Wire and Arc Additive Manufacturing (WAAM)," *Materials*, vol. 12, no. 7, 2019, doi: 10.3390/ma12071121.

[12] N. Chernovol, B. Lauwers, and P. van Rymenant, "Development of low-cost production process for prototype components based on Wire and Arc Additive Manufacturing (WAAM)," *Procedia CIRP*, vol. 95, pp. 60–65, 2020, doi: https://doi.org/10.1016/j.procir.2020.01.188.

[13] S. Williams and F. Martina, "Wire +arc additive manufacturing vs. traditional machining from solid: a cost comparison," 2015.

[14] Mathers G, "The Welding of Aluminium and Its Alloys", Accessed: Jul. 07, 2022. [Online]. Available: https://www.elsevier.com/books/the-welding-of-aluminium-and-its-alloys/mathers/978-1-85573-567-5

[15] R. Singh, "3 - Welding and joining processes," in *Applied Welding Engineering (Third Edition)*, R. Singh, Ed. Butterworth-Heinemann, 2020, pp. 157–186. doi: https://doi.org/10.1016/B978-0-12-821348-3.00015-X.

[16] S. W. Williams, F. Martina, A. C. Addison, J. Ding, G. Pardal, and P. Colegrove, "Wire + Arc Additive Manufacturing," *Materials Science and Technology*, vol. 32, no. 7, pp. 641–647, May 2016, doi: 10.1179/1743284715Y.0000000073.

[17] R. D. Valdemar, "DEVELOPMENTS IN DIRECTED ENERGY DEPOSITION ADDITIVE MANUFACTURING: IN-SITU HOT FORGING AND INDIRECT COOLING," 2022.

[18] E. Karayel and Y. Bozkurt, "Additive manufacturing method and different welding applications," *Journal of Materials Research and Technology*, vol. 9, no. 5, pp. 11424–11438, 2020, doi: https://doi.org/10.1016/j.jmrt.2020.08.039.

[19] S. Selvi, A. Vishvaksenan, and E. Rajasekar, "Cold metal transfer (CMT) technology - An overview," *Defence Technology*, vol. 14, no. 1, pp. 28–44, 2018, doi: https://doi.org/10.1016/j.dt.2017.08.002.

[20] R. D. Valdemar, "Additive manufacturing of a high resistance steel by MIG/MAG," 2016.

[21] P. Kah, H. Latifi, R. Suoranta, J. Martikainen, and M. Pirinen, "Usability of arc types in industrial welding," *International Journal of Mechanical and Materials Engineering*, vol. 9, no. 1, p. 15, 2014, doi: 10.1186/s40712-014-0015-6.

[22] E. F. da Silva, R. Jose, A. Scotti, and J. C. de Oliveira, "Power quality analysis of gas metal ARC welding process operating under different drop transfer modes," *XI Brazilian Power Electronics Conference*, pp. 129–135, 2011.

[23] D. Iordachescu, L. Quintino, R. Miranda, and G. Pimenta, "Influence of shielding gases and process parameters on metal transfer and bead shape in MIG brazed joints of the thin zinc coated steel plates," *Mater Des*, vol. 27, no. 5, pp. 381–390, 2006, doi: https://doi.org/10.1016/j.matdes.2004.11.010.

[24] F. Martina, P. A. Colegrove, S. W. Williams, and J. Meyer, "Microstructure of Interpass Rolled Wire + Arc Additive Manufacturing Ti-6Al-4V Components," *Metallurgical and Materials Transactions A*, vol. 46, no. 12, pp. 6103–6118, 2015, doi: 10.1007/s11661-015-3172-1.

[25] J. Gu, J. Ding, S. W. Williams, H. Gu, P. Ma, and Y. Zhai, "The effect of inter-layer cold working and post-deposition heat treatment on porosity in additively manufactured aluminum alloys," *J Mater Process Technol*, vol. 230, pp. 26–34, 2016, doi: https://doi.org/10.1016/j.jmatprotec.2015.11.006.

[26] J. R. Hönnige, P. Colegrove, and S. Williams, "Improvement of microstructure and mechanical properties in Wire + Arc Additively Manufactured Ti-6Al-4V with Machine Hammer Peening," *Procedia Eng*, vol. 216, pp. 8–17, 2017, doi: https://doi.org/10.1016/j.proeng.2018.02.083.

[27] V. R. Duarte, T. A. Rodrigues, N. Schell, R. M. Miranda, J. P. Oliveira, and T. G. Santos, "Hot forging wire and arc additive manufacturing (HF-WAAM)," *Addit Manuf*, vol. 35, p. 101193, 2020, doi: https://doi.org/10.1016/j.addma.2020.101193.

[28] B. Wu, Z. Pan, D. Ding, D. Cuiuri, H. Li, and Z. Fei, "The effects of forced interpass cooling on the material properties of wire arc additively manufactured Ti6Al4V alloy," *J Mater Process Technol*, vol. 258, pp. 97–105, 2018, doi: https://doi.org/10.1016/j.jmatprotec.2018.03.024.

[29] Z. Qi, B. Cong, B. Qi, H. Sun, G. Zhao, and J. Ding, "Microstructure and mechanical properties of double-wire + arc additively manufactured Al-Cu-Mg alloys," *J Mater Process Technol*, vol. 255, pp. 347–353, 2018, doi: https://doi.org/10.1016/j.jmatprotec.2017.12.019.

[30] J. P. Oliveira, T. G. Santos, and R. M. Miranda, "Revisiting fundamental welding concepts to improve additive manufacturing: From theory to practice," *Prog Mater Sci*, vol. 107, p. 100590, 2020, doi: https://doi.org/10.1016/j.pmatsci.2019.100590.

[31] Y. Zhang, Y. Chen, P. Li, and A. T. Male, "Weld deposition-based rapid prototyping: a preliminary study," *J Mater Process Technol*, vol. 135, no. 2, pp. 347–357, 2003, doi: https://doi.org/10.1016/S0924-0136(02)00867-1.

[32] Z. Hu, X. Qin, T. Shao, and H. Liu, "Understanding and overcoming of abnormity at start and end of the weld bead in additive manufacturing with GMAW," *The International Journal of Advanced Manufacturing Technology*, vol. 95, no. 5, pp. 2357–2368, 2018, doi: 10.1007/s00170-017-1392-9.

[33] K. Treutler and V. Wesling, "The Current State of Research of Wire Arc Additive Manufacturing (WAAM): A Review," *Applied Sciences*, vol. 11, no. 18, 2021, doi: 10.3390/app11188619.

[34] T. A. Rodrigues, V. Duarte, R. M. Miranda, T. G. Santos, and J. P. Oliveira, "Current status and perspectives on wire and arc additive manufacturing (WAAM)," *Materials*, vol. 12, no. 7, 2019, doi: 10.3390/ma12071121.

[35] R. Messler, "Weld Fusion Zone Solidification," 2007, pp. 373–453. doi: 10.1002/9783527617487.ch13.

[36] B. Wu *et al.*, "A review of the wire arc additive manufacturing of metals: properties, defects and quality improvement," *J Manuf Process*, vol. 35, pp. 127–139, 2018, doi: https://doi.org/10.1016/j.jmapro.2018.08.001.

[37] H. Zhang, Z. Xu, S. Yarmolenko, L. J. Kecskes, and J. Sankar, "Evolution of Microstructure and Mechanical Properties of Mg-6Al Alloy Processed by Differential Speed Rolling upon Post-Annealing Treatment," *Metals (Basel)*, vol. 11, no. 6, 2021, doi: 10.3390/met11060926.

[38] Peron Mirco, Berto Filippo, and Torgersen Jan, "Magnesium and Its Alloys as Implant Materials: Corrosion, Mechanical and Biological Performances".

[39] X. Cao, M. Jahazi, J. P. Immarigeon, and W. Wallace, "A review of laser welding techniques for magnesium alloys," *J Mater Process Technol*, vol. 171, no. 2, pp. 188–204, 2006, doi: https://doi.org/10.1016/j.jmatprotec.2005.06.068.

[40] Y. Guo, H. Pan, L. Ren, and G. Quan, "Microstructure and mechanical properties of wire arc additively manufactured AZ80M magnesium alloy," *Mater Lett*, vol. 247, pp. 4–6, 2019, doi: https://doi.org/10.1016/j.matlet.2019.03.063.

[41] J. Guo, Y. Zhou, C. Liu, Q. Wu, X. Chen, and J. Lu, "Wire Arc Additive Manufacturing of AZ31 Magnesium Alloy: Grain Refinement by Adjusting Pulse Frequency," *Materials*, vol. 9, no. 10, 2016, doi: 10.3390/ma9100823.

[42] H. Takagi *et al.*, "Material-property evaluation of magnesium alloys fabricated using wire-and-arc-based additive manufacturing," *Addit Manuf*, vol. 24, pp. 498–507, 2018, doi: https://doi.org/10.1016/j.addma.2018.10.026.

[43] T. Klein, A. Arnoldt, M. Schnall, and S. Gneiger, "Microstructure Formation and Mechanical Properties of a Wire-Arc Additive Manufactured Magnesium Alloy," *JOM*, vol. 73, no. 4, pp. 1126–1134, 2021, doi: 10.1007/s11837-021-04567-4.

[44] R. Singh, "3 - Welding and joining processes," in *Applied Welding Engineering (Third Edition)*, Third Edition., R. Singh, Ed. Butterworth-Heinemann, 2020, pp. 157–186. doi: https://doi.org/10.1016/B978-0-12-821348-3.00015-X.

[45] W. Xu *et al.*, "Dynamic wetting and spreading mechanisms regulated by elemental Ni in a Mg/steel immiscible system during laser processing," *J Manuf Process*, vol. 80, pp. 600–611, 2022, doi: https://doi.org/10.1016/j.jmapro.2022.06.042.

[46] "Standard Test Methods for Vickers Hardness and Knoop Hardness of Metallic Materials," *ASTM International E92 − 17*, 2017, doi: 10.1520/E0092-17.

[47] S. Gneiger, J. A. Österreicher, A. R. Arnoldt, A. Birgmann, and M. Fehlbier, "Development of a High Strength Magnesium Alloy for Wire Arc Additive Manufacturing," *Metals (Basel)*, vol. 10, no. 6, 2020, doi: 10.3390/met10060778.

[48] J. Guo, Y. Zhou, C. Liu, Q. Wu, X. Chen, and J. Lu, "Wire Arc Additive Manufacturing of AZ31 Magnesium Alloy: Grain Refinement by Adjusting Pulse Frequency," *Materials*, vol. 9, no. 10, 2016, doi: 10.3390/ma9100823.

[49] H. TENG, T. LI, X. ZHANG, and Z. ZHANG, "Influence of sub-rapid solidification on microstructure and mechanical properties of AZ61A magnesium alloy," *Transactions of Nonferrous Metals Society of China*, vol. 18, pp. s86–s90, 2008, doi: https://doi.org/10.1016/S1003-6326(10)60180-X.

[50] A. R. McAndrew *et al.*, "Interpass rolling of Ti-6Al-4V wire + arc additively manufactured features for microstructural refinement," *Addit Manuf*, vol. 21, pp. 340–349, May 2018, doi: 10.1016/j.addma.2018.03.006.

⟨year⟩ JOHN DOE A VERY LONG AND IMPRESSIVE THESIS TITILE WITH A FORCED LINE NOVA SCHOOL OF SCIENCE & TECHNOLOGY